UNITED STATES
NUCLEAR REGULATORY COMMISSION
WASHINGTON, D. C. 20555

AUG 15 1984

Docket No.: 50-395

APPLICANT: South Carolina Electric & Gas Company

FACILITY: V. C. Summer Nuclear Station

SUBJECT: SUMMARY OF MEETING WITH SOUTH CAROLINA ELECTRIC & GAS COMPANY

GENERAL

On July 25, 1984, the NRC staff met with South Carolina Electric and Gas Company (SCE&G) to discuss the structural analysis performend for the rerack of the spent fuel pool. The meeting was held in Bethesda, Maryland. A list of those persons who attended the meeting is included as Enclosure 1.

DISCUSSION

SCE&G made a presentation concerning the structural analysis performed for the rerack and their refueling schedule. Specifically, for the structural analysis, the hydrodynamic mass and the convergence of the solution were discussed.

Enclosure 2 is a copy of the view-graphs used at the meeting. Enclosures 3 and 4 are copies of 2 papers handed out at the meeting.

CONCLUSION

The NRC staff stated that they needed additional information submitted with respect to the hydrodynamic mass, the convergence of the solution, and the stress analysis of the dropped fuel accident. SCE&G stated that they would submit additional information on these subjects.

Jon Hopkins, Project Manager
Licensing Branch No. 4
Division of Licensing

Enclosure:
As stated

cc: See next page

SUMMER

Mr. O. W. Dixon, Jr.
Vice President, Nuclear Operations
South Carolina Electric & Gas Company
P.O. Box 764 (Mail Code F-04)
Columbia, South Carolina 29218

cc: Senior Vice President
     South Carolina Public Service Authority
     223 North Live Oak Drive
     Moncks Corner, South Carolina 29461

     J. B. Knotts, Jr., Esq.
     Bishop, Liberman, Cook, Purcell
       and Reynolds
     1200 17th Street, N.W.
     Washington, D. C. 20036

     Mr. Mark B. Whitaker, Jr.
     Group Manager - Nuclear Engineering
       & Licensing
     South Carolina Electric & Gas Company
     P.O. Box 764
     Columbia, South Carolina 29218

     Resident Inspector/Summer NPS
     c/o U.S. Nuclear Regulatory Commission
     Route 1, Box 64
     Jenkinsville, South Carolina 29065

     James P. O'Reilly, Regional Administrator
     U.S. Nuclear Regulatory Commission,
       Region II
     101 Marietta Street, N.W., Suite 2900
     Atlanta, Georgia 30323

ATTENDEES JULY 25, 1984 MEETING

NRC

J. Hopkins

G. Lear

P. Kuo

S. Kim

O. Rothberg

J. Lombardo

C. Herrick - Consultant (FRC)

T. Belytschko - Consultant

SCE&G

D. Nauman

N. Clark

A. Monroe

O. Dixon

Joseph Oat Corporation

K. Singh

"OT POSITION FOR REVIEW AND ACCEPTANCE OF SPENT FUEL STORAGE AND HANDLING APPLICATIONS"

USNRC (1978-79)

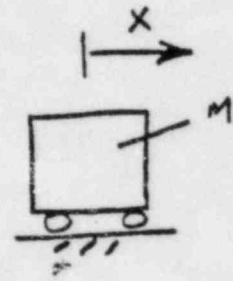SECTION IV   PARAGRAPH (3)

"THE PEAK RESPONSE FROM EACH DIRECTION SHOULD BE COMBINED BY THE SQUARE ROOT OF THE SUM OF THE SQUARES"

----- ALSO IN NUREG-0800
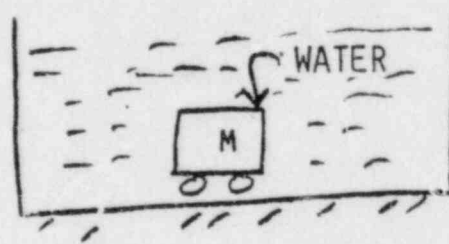
(I)   ISOLATED BODY

MASS X ACCN = EXTERNAL FORCE

$$M \frac{D^2X}{DT^2} = F$$

(II)   ISOLATED BODY IN WATER

$$(M + M_V) \frac{D^2X}{DT^2} = F$$
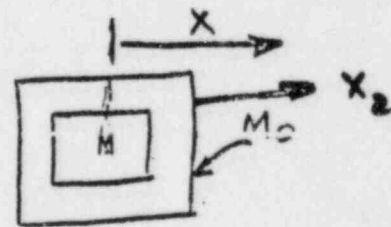
M_V = VIRTUAL MASS

(III)   PROXIMATE BODIES

$$(M + M_V) \ddot{X} + M_H \ddot{X}_2 = F$$

M_V = VIRTUAL MASS

M_H = HYDRODYNAMIC MASS

STANDARD SOLUTION

R.J. FRITZ, "THE EFFECT OF LIQUIDS ON THE DYNAMIC MOTIONS OF IMMERSED SOLIDS", JOURNAL OF ENGINEERING FOR INDUSTRY (1972)

$$M_H \approx 1/GAP$$

HOW ACCURATE IS THE SOLUTION FOR RATTLING FUEL ASSEMBLIES??

GENERALIZED SOLUTION [SOLER & SINGH (1981)]

$$Q_{F_1} = M_1 (\ddot{X}_1 - \ddot{Y}_1) + \frac{\Psi_1}{3} (\dot{X}_1 - \dot{Y}_1)^2$$

$$+ \Psi_2 (\dot{X}_1 - \dot{Y}_1)(\dot{X}_2 - \dot{Y}_2) - \frac{\Psi_1}{2} (\dot{X}_2 - \dot{Y}_2)^2$$

$$Q_{F_2} = M_2 (\ddot{X}_2 - \ddot{Y}_2) + \frac{\Psi_2}{6} (\dot{X}_2 - \dot{Y}_2)^2$$

$$+ \frac{\Psi_1}{6} (\dot{X}_1 - \dot{Y}_1)(\dot{X}_2 - \dot{Y}_2) - \frac{\Psi_2}{6} (\dot{X}_1 - \dot{Y}_1)^2$$

WHERE:

$$\Psi_I = \frac{P C^3 L}{H^2} \cdot \frac{\mathcal{E}_I}{(1 - \mathcal{E}_I^2)^2} \quad ; \quad I = 1,2$$

$$M_I = \frac{P C^3 L}{2 H} \left[\frac{1}{3(1 - \mathcal{E}_I)^2} + \frac{1}{(1 - \mathcal{E}_j)^2} \right]$$

$$I = 1, \quad J = 2$$
$$I = 2, \quad J = 1$$

$$\mathcal{E}_I = (X_I - Y_I) / H$$
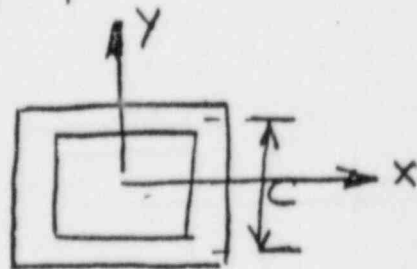
TEST PROBLEM -- BWR FUEL RACKS

CASE	MAXIMUM FLOOR LOAD (NEWTON'S)
1. NO WATER	2.67×10^6
2. FRITZ WITH DAMPING	2.228×10^6
3. GENERALIZED SOLN WITHOUT DAMPING	1.997×10^6
4. GENERALIZED SOLN WITH DAMPING	1.535×10^6
5. GENERALIZED SOLN WITH 1% OF COMPUTED DAMPING	1.766×10^6

CONCLUSION:

WITHOUT FORM DRAG EFFECTS: GENERALIZED SOLN GIVES AT LEAST 25%
REDUCTION IN COMPUTED FLOOR LOAD

Typical Solution

Max. disb. (y-axis)

→ _P size_ (x-axis)
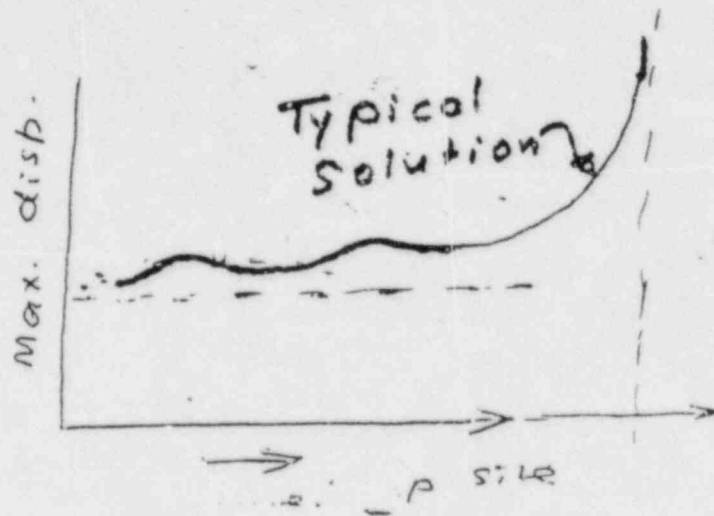
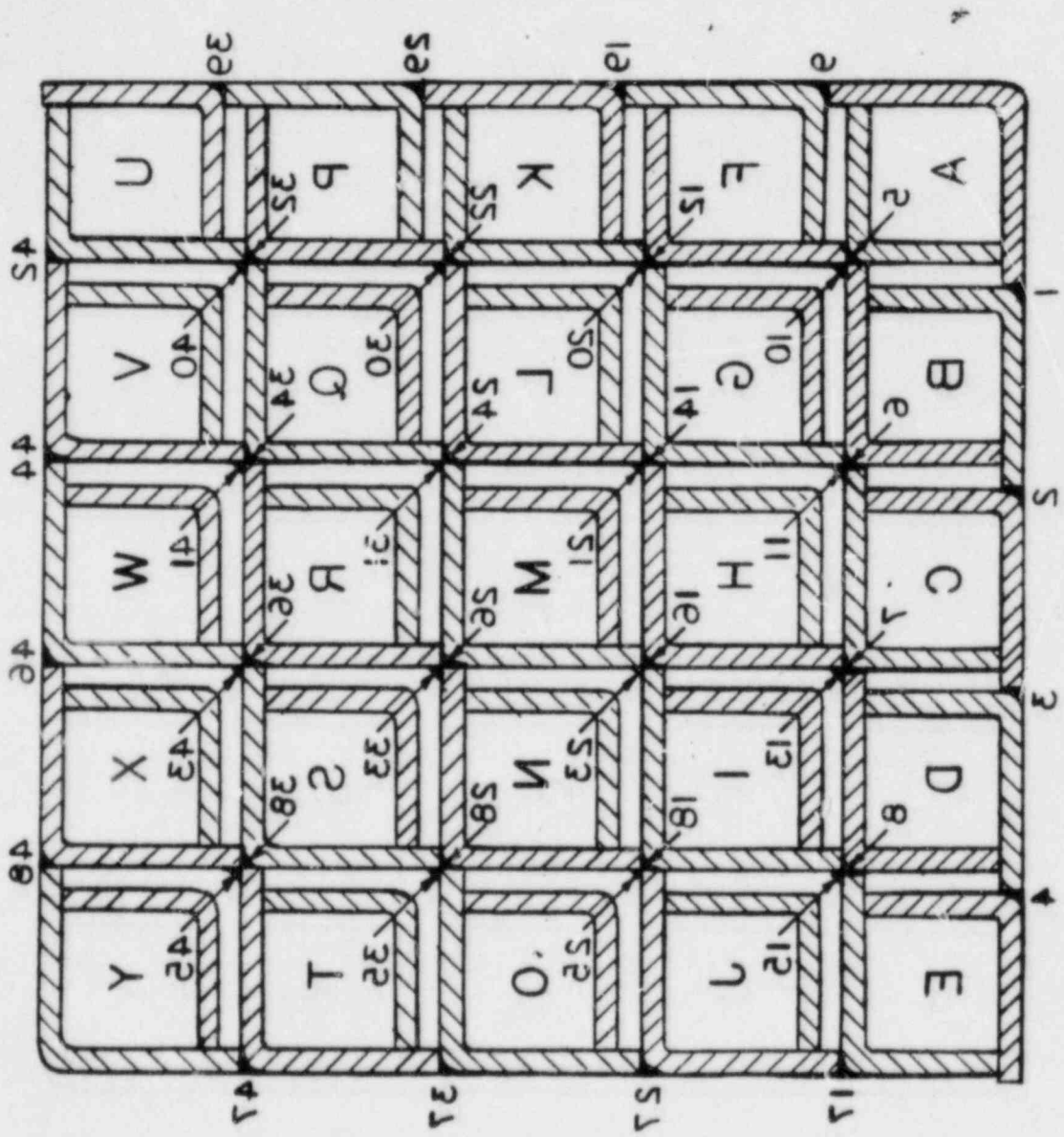| TIME INCREMENT (Secs)	DISPLACEMENT
$.4 \times 10^{-4}$	@ .0059 sec
$.325 \times 10^{-4}$	@ .0131 sec
~~████~~	~~████~~
0.3	1.298" @ 13.73 sec
0.2	0.17" @ ≈ 5 sec
0.2	≈ 0.8" [TWO DIMENSIONAL LOADING]

FIG. 3.4.4 COMPOSITE BOXES WELDING SEQUENCE OF
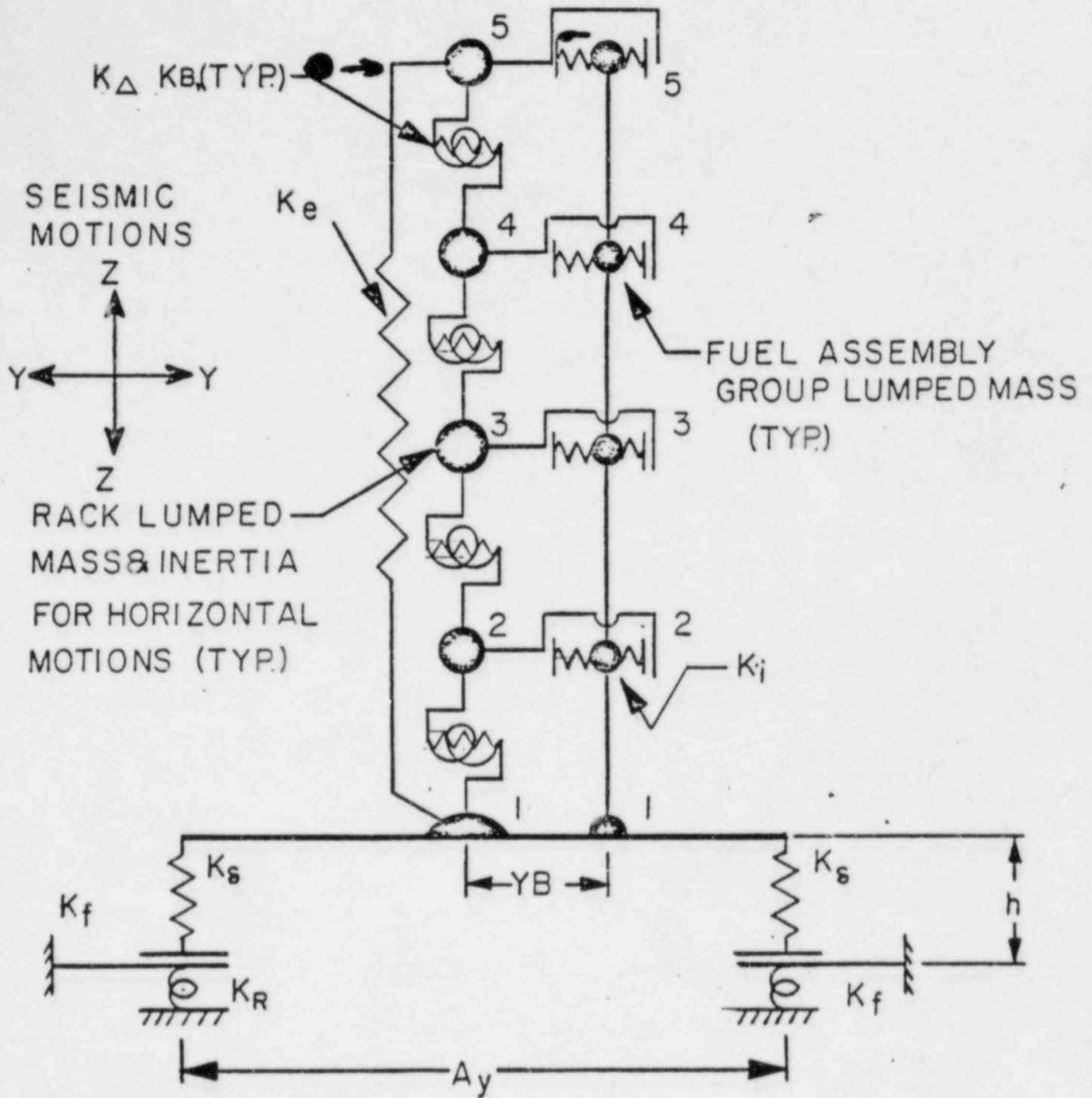
FIG. 6.3 SPRING MASS SIMULATION FOR A TWO DIMENSIONAL MOTION

X_B, Y_B = OFFSET OF FUEL ASSEMBLY GROUP CENTROID FROM RACK MODULE CENTER.
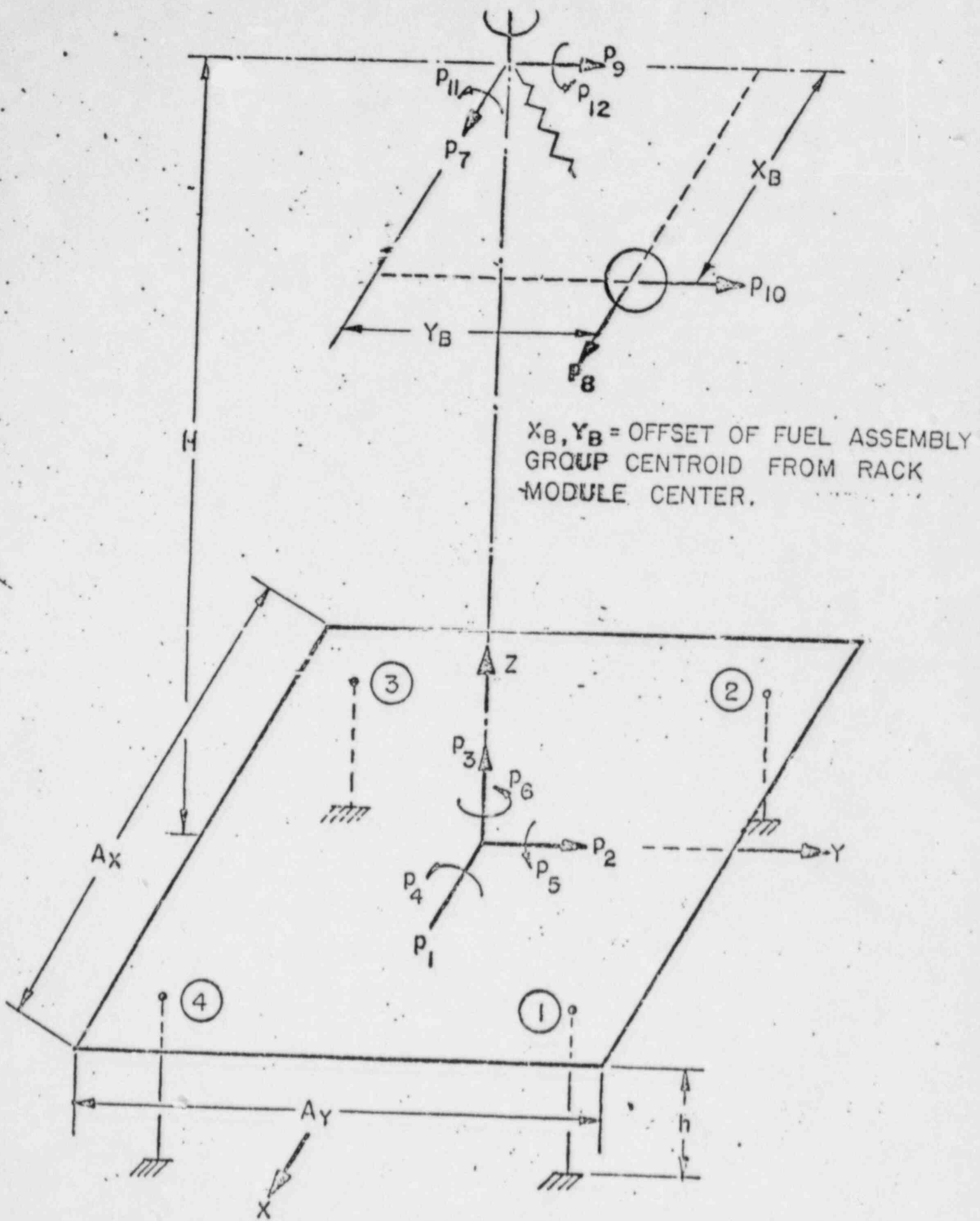
FIG. 1: RACK MODEL SHOWING DEGREES OF FREEDOM
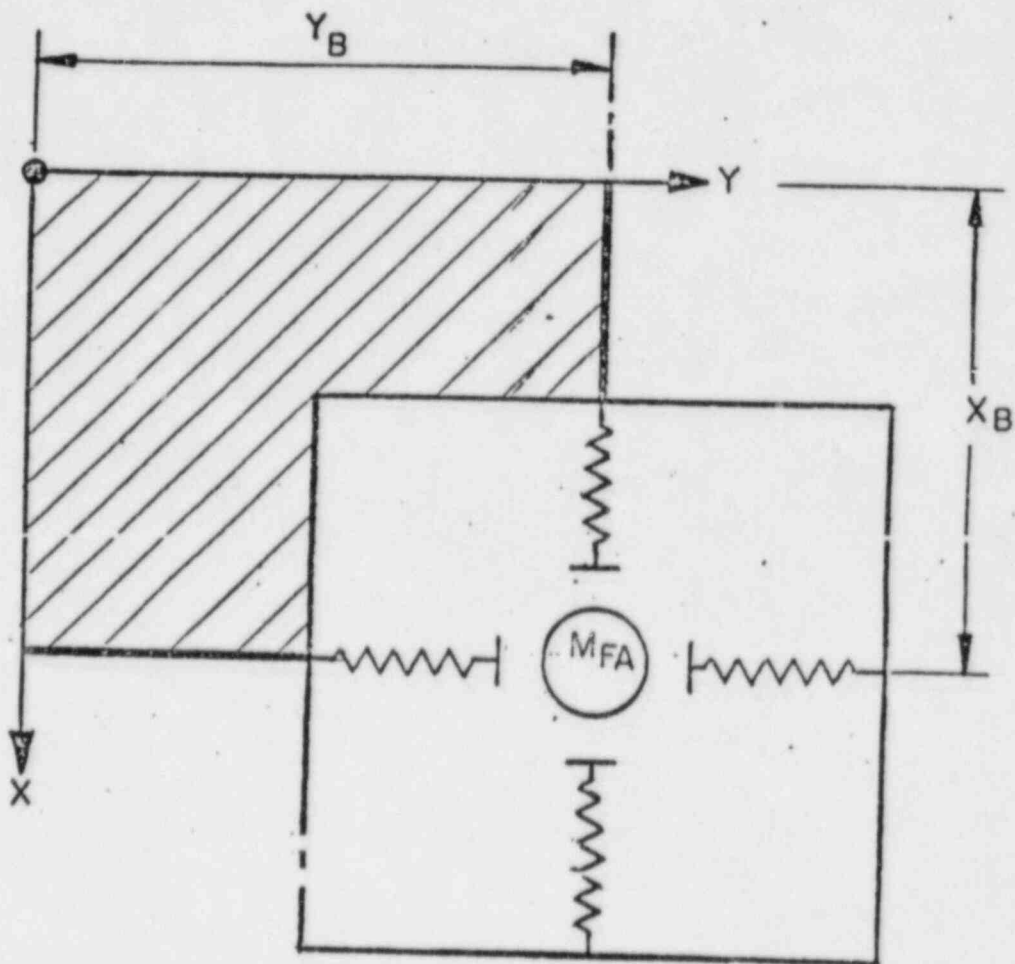
FIG. 2; IMPACT SPRING ORIENTATION AT TOP OF RACK

14 DEGREE-OF-FREEDOM RUN

RACK F - GPU OYSTER CREEK PLANT

ASSUMPTION:

1. 4% STRUCTURAL DAMPING

2. NO FORM DRAG

3. ASSEMBLIES VIBRATE IN UNION.

4. NO ADDITIONAL DAMPING OF THE FUEL ASSEMBLY IMPACT LOCATION.

5. SAFE SHUTDOWN EARTHQUAKE - IN X-DIRECTION, AND VERTICAL EARTHQUAKE

6. 5/8" SIDE GAP

CONVERGENCE RUNS

FILE NAME	TIME STEP (SECS)	MAXIMUM DISPLACEMENT TOP (INCH)	BOTTOM (INCH)
DGPT60	.0003	.6631	.000952
DGPT61	.0002	.6631	.0009517
DGPT62	.0001	.6631	.0009517

CONCLUSION: CONVERGENCE IS COMPLETE AND TOTAL

REV.

120 $\frac{5}{32}$" REF.

REGION 3 11 X 11	REGION 1 11 X 11	REGION 3 11 X 11	RESERVED AREA
REGION 3 11 X 11	REGION 1 11 X 11	REGION 3 11 X 11	REGION 3 11 X 11
REGION 3 11 X 10	REGION 2 11 X 9	REGION 3 11 X 10	REGION 3 11 X 10

5" REF.

6 $\frac{1}{8}$" REF.

5" REF.

117 $\frac{11}{16}$" REF.

110 $\frac{13}{16}$"

7 $\frac{7}{8}$"

1 $\frac{7}{8}$"

100 $\frac{5}{8}$"

5"

1 $\frac{1}{4}$"

114 $\frac{1}{4}$"

1 $\frac{7}{8}$"

9 $\frac{1}{2}$"

6 $\frac{1}{8}$"

5"

110 $\frac{13}{16}$"

110 $\frac{13}{16}$"

100 $\frac{5}{8}$"

1 $\frac{7}{8}$"

5"

28'-0"

110 $\frac{13}{16}$"   114 $\frac{1}{4}$"   110 $\frac{13}{16}$"   110 $\frac{13}{16}$"

6 $\frac{23}{32}$"   2 $\frac{5}{8}$"   2 $\frac{5}{8}$"   2 $\frac{5}{8}$"   6 $\frac{23}{32}$" REF.

39'-0"

2-5
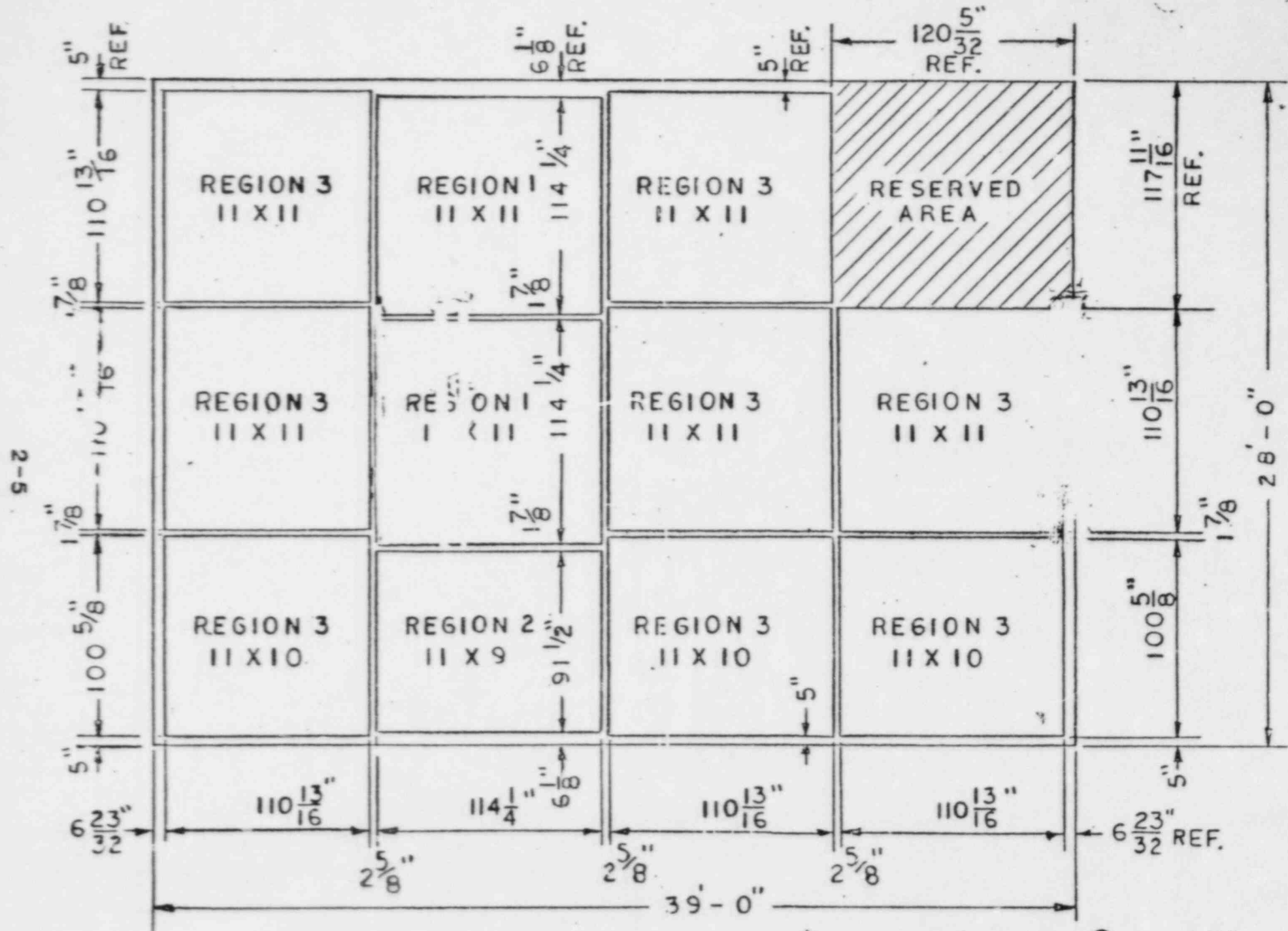
FIG. 2·1   MODULE LAYOUT   V. C. Summer

<u>V.C. SUMMER RESULTS</u>

RACK I.D.	X-DISPLACEMENT		Y-DISPLACEMENT	
	ACTUAL	LIMIT	ACTUAL	LIMIT
REGION II 11 x 9	0.74"	0.94" (1 7/8")	1"	1.313" (2 5/8")
REGION I 11 x 11	0.78"	0.94" (1 7/8")	0.86"	1.313" (2 5/8")

- The rack modules develop stresses which are <u>a fraction of The permissible limits.</u>

- Racks can not be built any more rigid with The amount of material utilized.

DYNAMIC COUPLING IN A CLOSELY SPACED TWO-BODY SYSTEM

VIBRATING IN A LIQUID MEDIUM: THE CASE OF FUEL RACKS

A.I. SOLER

Professor of Mechanical Engineering and Applied Mechanics

University of Pennsylvania, Philadelphia, PA, 19104 U.S.A.

K.P. SINGH

Vice President Engineering, Joseph Oat Corporation,

2500 Broadway, Camden, NJ 08104 U.S.A.

SUMMARY

An approximate analysis of the effects of confined fluid on the mass
and damping present in high density spent fuel storage racks is performed.
It is shown that inclusion of large displacement effects is required to
yield realistic results for rack forces and pool floor slab forces. The
theory is developed for square cell geometries, and a simple two degree of
freedom numerical example is presented to illustrate the effects.

NOMENCLATURE

c	:	Characteristic dimension of gap (Fig. 2)
f^s	:	Friction Coefficient (Eq. 16)
h	:	Nominal gap between body 1 and body 2 (Fig. 2)
h_i	:	Gap in annulus i at time t. (Fig. 1)
K	:	Loss coefficient
K_f	:	Kinetic energy of the fluid set in motion
L	:	Length of bodies 1 and 2 (dimension perpendicular to the plans of motion)
p_i	:	Hydrostatic pressure in gap i.
Q_{f1}, Q_{f2}	:	Generalized forces corresponding to system Lagrangian in X and Y directions, respectively.

S_i	:	Length co-ordinate in gap i.
U_1	:	Displacement of body 1 (inner body) in X-direction (Fig. 2)
U_2	:	Displacement of body 1 (inner body) in Y-direction (Fig. 2)
V_1	:	Displacement of body 2 in X-direction (Fig. 2)
V_2	:	Displacement of body 2 in Y-direction (Fig. 2)
W_i	:	Width of gap i at time t (Eq. 3)
$\dot{Z}_+, \dot{Z}_-$	:	Velocity of body inner and outer bodies, respectively.
ϵ_i	:	Dimensionless width of gap i
μ	:	Ratio of length to nominal width of gap (Eq. 7)
ρ	:	Mass density of the fluid medium.

INTRODUCTION

1.   Dynamic coupling between proximate bodies vibrating in a fluid medium is a well known phenomenon [1]. In the special case of a two body system executing planar motion where one body is completely enveloped by another, Fritz [2] derived expressions for the virtual mass and the couplant inertial force under the assumption that the motions are of small amplitude. Fritz's work has been the basis of the dynamic modelling of fluid coupling in much of the structural analysis performed in the nuclear industry [3]. Dong [4] gives a concise account of previously published work on dynamic coupling between closely spaced bodies executing small amplitude motions. Unfortunately, the assumption of infinitesimal vibrations is rather untenable in many applications. The case of "poisoned"* fuel storage racks containing spent nuclear fuel is one such example. The fuel rack dynamic coupling problem will be described in some detail since it provided the primary impetus for this study.

*   The term "poison" denotes a product containing the B^{10} isotope, used for capturing neutrons.

2.   A "poisoned" or high density storage rack is essentially an assemblage of cellular members of square cross sectional openings. Fuel storage racks are about 16' (4.88 m.) high and vertically submerged in fuel pools containing approximately 40' of water. Spent fuel assemblies, after their removal from the reactor core, are placed in these cellular locations for long term radioactive decay.

3.   Figure 1 shows a typical channelled BWR fuel assembly in a storage cell. Curbs on fuel reprocessing have accentuated utilities' need to use "poisoned" storage racks, as opposed to open lattice construction employed in the past. Water in the pool acts to moderate the emitted neutrons and to transport the spent fuel decay heat. However, in the event of an earthquake, it also produces dynamic coupling between the fuel assembly and

the cellular container around it. The gap between the fuel assembly and the container is in the order of 0.006-0.008 m. on each side. For example, the cells for BWR fuel assemblies (approximately 0.133 m side dimension) are typically made 0.1524 m square. When subjected to a given ground motion, a fuel assembly is free to vibrate and local impacts with the storage cell may occur. The magnitude of impact, of course, is a strong function of the dynamic coupling between the vibrating fuel assembly and its surrounding vibrating fuel cell. A multitude of fuel vibrating in unison and impacting storage containers can yield a large overturning force on the storage racks. Ultimately, this load must be borne by the pool floor slab, and its supporting structure. Moreover, in free-standing racks (unanchored to the floor), excessive rigid body displacement of the rack, and consequent inter-rack impact are also areas of concern. These considerations indicate the importance of modelling the fuel assembly/cell dynamic coupling in an appropriate manner. This is especially important in operating plants, since strengthening of their pool floor and support structure is all but impossible in most cases. It is important to develop a seismic model that yields conservative results for floor slab forces, yet is not so conservative that unrealistically high floor loads are obtained.

4. It is recognized that the velocity of water in the gap between the fuel assembly and the storage cell will be three dimensional. However, the axial component will be quite small since the length of the fuel assembly is an order of magnitude greater than the characteristic gap dimension. Thus it is sufficiently accurate to model the problem in two dimensions as shown in Figure 2. The outer body of square cross sectional opening simulates a single storage cell. The fuel assembly is modelled as an unperforated square cross-section to simulate a channeled BWR fuel assembly. It is intuitively obvious that the effect of elastic deformation of the cell and channel walls on the fluid motion will be insignificant. Therefore, the walls of the two bodies are assumed to be rigid. For analysis, the inner body is labelled as body 1, and the outer body is labelled as body 2. The fluid inertia forces on body 1 due to an imposed two dimensional motion on body 2 are determined by writing the system Lagrangian for the fluid kinetic energy assuming inviscid flow. Lagrange's equations of motion are used to determine the generalized force. The amplitude of oscillations of the inner body (body 1) is allowed to be comparable in magnitude to the inter-body gap. The resulting expression shows that the dynamic coupling consists of a virtual mass, a coupling inertial mass of the type derived by Fritz, and an additional non-linear force which may be referred to as "fluid spring". These three forces completely characterize the fluid forces for large amplitude motion under inviscid conditions. Fluid damping due to duct flow type losses due to form drag can also be derived from force equilibrium, if the duct turnaround coefficients are known. Expressions for equivalent damping due to drag are also given here for the sake of completeness.

5. In the following section, the detailed analysis of the subject problem is given. The results of the analysis are illustrated by treating a typical numerical problem in some detail. The primary intent of this analysis is to demonstrate that accurate determination of fluid effects requires inclusion of the effect of motions that are large compared to the gap between fuel assembly and cell walls. To illustrate the potential effects, a simple two degree of freedom model is subjected to a simulated seismic event, and a comparison between small and large displacement

solutions is made to illustrate errors sustained in using the small displacement theory.

Approximate Analysis of Duct Flow

6. We consider the 2-D cross section shown in Figure 2. Neglecting out-of-plane flow, and assuming small gap width h_i compared to the characteristic length c, permits the incompressible flow continuity equation to be written, in each portion of the duct, as

$$\frac{\partial \dot{u}_i}{\partial S_i} = \frac{-\dot{Z}_+ - \dot{Z}_-}{h_i} \tag{1}$$

which yields the solution for the local fluid velocity

$$\dot{U}_i = -\frac{\left(\dot{Z}_+ - \dot{Z}_-\right)}{h_i} S_i + B_i(t) \tag{2}$$

In terms of displacements $U_i(t)$, $V_i(t)$, $i = 1, 2$ shown in Figure 2, we define

$$W_i = U_i - V_i ; \qquad \epsilon_i = W_i(t) / h h ; i = 1, 2 \tag{3}$$

If h is defined as the nominal gap width around the entire periphery, then the current gap widths in any portion of the cross section are given by the relations

$$h_{1,3} = h \, (1 \mp \epsilon_1) ; h_{2,4} = h (1 \mp \epsilon_2) \tag{4}$$

Applying Equation (2) to each region, and interpreting S_i as either x or y, $\dot{Z}_+ = \pm \dot{U}_i$, $\dot{Z}_- = \pm \dot{V}_i$, yields

$$\dot{u}_1 = \dot{W}_1 y/h_1 + B_1(t) ; \dot{u}_2 = -\dot{W}_2 x/h_2 + B_2(t)$$
$$\dot{u}_3 = \dot{W}_1 y/h_3 + B_3(t) ; \dot{u}_4 = -\dot{W}_2 x/h_4 + B_4(t) \tag{5}$$

At corners, we require flow continuity in the local S_i direction and impose the following conditions to determine $B_i(t)$;

$$h_1 u_1 (^c/2) = h_2 u_2(^c/2) ; h_2 u_2(- _2) = h_3 U_3 (_c/2)$$
$$h_3 u_3(-^c/2) = h_4 U_4(-^c/2); h_4 u_4(^c/2) = h_1 U_1(-^c/2) \tag{6}$$

where $u_i \, (^c/2)$ denotes u_i evaluated at $S = \frac{c}{2}$ in region 1.

7. The following final solutions are obtained for the approximate flow velocity distribution.

$$U_1(S,t) = \frac{-\mu \dot{W}_2}{2(1-\epsilon_1)} + \frac{\mu \dot{W}_1}{(1-\epsilon_1)} \, Y/_c ; \mu = {}^c/_h$$

$$U_2(S,t) = \frac{\mu \dot{W}_1}{2(1-\epsilon_2)} - \frac{\mu \dot{W}_2}{(1-\epsilon_2)} \, x/_c \tag{7}$$

$$U_3(S,t) = \frac{\mu \dot{W}_2}{2(1+\epsilon_1)} + \frac{\mu \dot{W}_1}{(1+\epsilon_1)} \, Y/_c$$

818

$$U_4(S,t) = \frac{-\mu \dot{W}_1}{2(1+\varepsilon_2)} - \frac{\mu \dot{W}_2}{(1+\varepsilon_2)} \, x/c$$

The kinetic energy of the fluid can be written in the form

$$K_f = \sum_{i=1}^{4} \int_{-\frac{c}{2}}^{c/2} \frac{\rho \, h_i}{2} \, (\alpha_i + \beta_i \, S_i/c)^2 \, S \, d_i \, L \qquad (8)$$

where we have temporarily employed the notation $u_i = \alpha_i + \beta_i \, S_i/c$ and L is the length of the container. integrating yields

$$K_f = \sum_{i=1}^{4} \frac{\rho \, h_i}{2} \left[\alpha_i^2 + \frac{\beta_i^2}{12} \right] C \, L \qquad (9)$$

After eliminating α_i, β_i by inspection of Equation (7), we obtain

$$K_f = \frac{\rho \, C^3 L}{8 \, h} \left[\phi_1 \, \dot{W}_1^2 + \phi_2 \, \dot{W}_2^2 \right] \qquad (10)$$

with

$$\phi_1 = \frac{2}{3(1-\varepsilon_1^2)} + \frac{2}{(1-\varepsilon_2^2)}$$

$$\phi_2 = \frac{2}{3(1-\varepsilon_2^2)} + \frac{2}{(1-\varepsilon_1^2)} \qquad (11)$$

We form

$$Q_{fi} = \frac{d}{dt} \left(\frac{\partial K_f}{\partial \dot{W}_i} \right) - \frac{\partial K_f}{\partial W_i} \quad ; \quad i = 1, 2$$

and obtain the formal results

$$\frac{Q_{f1}}{L} = \frac{\rho \, C^3}{4 \, h} \phi_1 \, \ddot{W}_1 + \frac{\rho \, C^3}{4 \, h} \dot{W}_1 \left(\frac{\partial \phi_1}{\partial W_1} \, \dot{W}_1 + \frac{\partial \phi_1}{\partial W_2} \, \dot{W}_2 \right)$$

$$- \frac{\rho \, C^3}{8 \, h} \frac{\partial \phi_1}{\partial W_1} \, \dot{W}_1^2 + \frac{\partial \phi_2}{\partial W_1} \, \dot{W}_2^2 \qquad (12)$$

$$\frac{Q_{f2}}{L} = \frac{\rho \, C^3}{4 \, h} \phi_2 \, \ddot{W}_2 + \frac{\rho \, C^3}{4 \, h} \dot{W}_2 \left(\frac{\partial \phi_2}{\partial W_1} \, \dot{W}_1 + \frac{\partial \phi_2}{\partial W_2} \, \dot{W}_2 \right)$$

$$- \frac{\rho \, C^3}{8 \, h} \left(\frac{\partial \phi_1}{\partial W_2} \, \dot{W}_1^2 + \frac{\partial \phi_2}{\partial W_2} \, \dot{W}_2^2 \right)$$

8. Using Equation (11) to evaluate $\partial \phi_i / \partial W_i$ permits us to finally write Q_{fi} as

$$Q_{f1} = m_1 \ddot{W}_1 + \frac{\psi_1}{6} \dot{W}_1^2 + \psi_2 \dot{W}_1 \dot{W}_2 - \frac{\psi_1}{2} \dot{W}_2^2$$

$$Q_{f2} = m_2 \ddot{W}_2 + \frac{\psi_2}{6} \dot{W}_2^2 + \psi_1 \dot{W}_1 \dot{W}_2 - \frac{\psi_2}{2} \dot{W}_1^2$$

(13)

where

$$\psi_i = \frac{\rho \, C^3}{h^2} L \, \frac{\varepsilon_i}{(1-\varepsilon_i^2)^2} \quad ; \quad i = 1,2$$

(14)

$$m_i = \frac{\rho \, C^3}{2h} L \left[\frac{1}{3(1-\varepsilon_i^2)} + \frac{1}{(1-\varepsilon_j^2)} \right] \begin{matrix} i=1 \ , j=2 \\ i=2 \ , j=1 \end{matrix}$$

(15)

9. Equations (13) and (15) provide the contribution of the fluid in the gap to the system Lagrangian and includes all conservative effects. We clearly see the virtual mass effects in the leading terms of Equation (13). The coupled quadratic terms in the generalized velocities appear solely from the assumption that ε_i need not be small compared to unity. For small vibrations, with $\varepsilon_i \rightarrow 0$, then $\psi_i \rightarrow 0$, and $m_i \rightarrow \frac{2}{3} \rho \, c^3 L/h$. It should be noted that the quadratic terms in Equation (13) do not behave as velocity squared damping terms, but appear to behave more like non-linear springs. This is easily seen by considering the uni-directional motion case with $W_1 = 0$. It is clear, there, that the term $\frac{\psi_2}{6} \dot{W}_2^2$ changes sign only when ε_2 changes sign; that is, no net energy is dissipated during a complete harmonic motion cycle.

10. The usual small motion analysis includes only the virtual mass effects; the effect of fluid friction can be shown to be negligible. In our case, where large motions, relative to the nominal gap width h, are admissible, we need to compute additional contributions to Equation (13) which account for frictional forces and the turning losses. The following approximate analysis is used to develop the additional terms necessary to include dissipative effects.

11. If the balance between pressure and frictional shear forces along any straight portion of the duct is considered, Reference 5 shows that the governing relation for the fluid pressure change due to shear stress is

$$\frac{\partial P}{\partial S_i} = -2 \frac{\tau_{fi}}{h_i} = -\frac{f^* \rho \, U_i |U_i|}{h_i}$$

(16)

where f* is the friction loss factor defined by the relation

$$\tau_{fi} = \frac{f^*}{2} \rho \, U_i |U_i|$$

12. Equation (10), written for each portion of the duct, can be integrated to yield the pressure distribution in each region. Note, however, that for arbitrary 2-D motions, proper attention must be focussed on the local fluid flow direction in each duct in order to ascertain the location of points of flow reversal. The arbitrary time functions arising from the integration of Equation (16) are determined by applying corner pressure matching conditions. From Figure 3, for i, j combinations 1,2 : 2,3: 3,4 : 4,1,

empirical equations for pressure loss due to abrupt turning of the flow may be written as:

$$\frac{P_j - P_i}{\rho} = -\frac{K}{2} V_m \left| V_m \right| \quad ; \quad 2V_m = U_i + U_j \tag{17}$$

where K is a loss coefficient.

13. For a general 2-D motion ($\dot{W}_1$, $\dot{W}_2 \neq 0$), the pressure in each region is fully determined by using Equations (16) and (17); contributions to the generalized forces Q_{fi} (Equation (13)), due to frictional and turning losses, are calculated from the expressions

$$F_x = L \int_{-c/2}^{c/2} (P_3 - P_1) \, dy$$

$$F_y = L \int_{-c/2}^{c/2} (P_4 - P_2) \, dx \tag{18}$$

Note that the direct effect of shear forces is neglected in Equation (18).

14. For the purpose of illustration, we restrict further damping computations to uni-directional motion, say $\dot{W}_2 \neq 0$. It is clear that the plane $x = 0$ is a plane of symmetry for the fluid flow; for such a motion, the pressure distribution due to friction losses in regions 2, 1, 4 in Figure 2 are obtained from Equation (16) as

$$P_2(x,t) = \frac{\rho \, f^* \, \mu^2 \, x^3 \, \dot{W}_2 \left| \dot{W}_2 \right|}{3 \, c^2 \, h \, (1-\epsilon_2)^3} + A_2(t) \quad ; \quad x \geqslant 0$$

$$P_1(y,t) = \frac{\rho \, f^* \, \mu^2 \, \dot{W}_2 \left| \dot{W}_2 \right| y}{4 \, h} + A_1(t) \quad ; \quad y \leqslant \frac{c}{2} \tag{19}$$

$$P_4(x,t) = \frac{\rho \, f^* \, \mu^2 \, x^3 \, \dot{W}_2 \left| \dot{W}_2 \right|}{3 \, c^2 \, h \, (1-\epsilon_2)^3} + A_4(t) \quad ; \quad x \geqslant 0$$

Using Equation (18) to compute F_y yields

$$F_y = 2L \int_0^{c/2} (P_4 - P_2) \, dx = \frac{\rho \, f^* \, \mu^3 \, C \, L \, \dot{W}_2 \left| \dot{W}_2 \right|}{96}$$
$$\left[\frac{1}{(1+\epsilon_2)^3} + \frac{1}{(1-\epsilon_2)^3} \right] + (A_4 - A_2) \, C \, L \tag{20}$$

Using Equation (19), and Equation (7) in Equation (17) at the corners $x = c/2$, $y = \pm c/2$ yields:

$$\frac{A_2-A_1}{\rho} = \frac{\mu^2 \dot{W}_2 \dot{W}_2}{8} \left\{ \frac{K}{4} \frac{(2-\epsilon_2)^2}{(1-\epsilon_2)^2} + \mu f^* \left[1 + \frac{1}{3(1-\epsilon_2)^3} \right] \right\}$$

$$\frac{A_1-A_4}{\rho} = \frac{\mu^2 \dot{W}_2 \dot{W}_2}{8} \left\{ \frac{K}{4} \frac{(2+\epsilon_2)^2}{(1+\epsilon_2)^2} + \mu f^* \left[1 + \frac{1}{3(1+\epsilon_2)^3} \right] \right\} \quad (21)$$

15. Solving Equation (21) for $\dfrac{A_2-A_4}{\rho}$ and substituting in Equation (20) yields the resulting velocity squared non-linear damping force as

$$F_y = c^*(\epsilon_2) \dot{W}_2 \left| \dot{W}_2 \right|$$

where

$$c^*(\epsilon_2) = \frac{\rho \mu^2 C L}{4} \left\{ \mu f^* \left[1 + \frac{(1+3\epsilon_2^2)}{4(1-\epsilon_2^2)^3} \right] \right\} + \frac{K}{4} \frac{[4-3\epsilon_2^2+\epsilon_2^4]}{(1-\epsilon_2^2)^2} \quad (22)$$

Dynamic Analysis

16. The simple dynamic model shown in Figure 4 is now considered as a vehicle to obtain numerical results which illustrate the effects of the fluid coupling. Linear springs K_I, K_o are introduced representing the elastic stiffness coupling the structure to ground, lumped masses M_I, M_O representing the mass of the respective solid bodies, and non-linear elements F_2^*, F_4^* which act only when impact between the bodies occurs. Then if $Y(t)$ represents a known ground motion, and relative co-ordinates U, v are introduced by the relations

$$U_2 = U + Y \; ; \; V_2 = v + Y \quad (23)$$

the equations of motion for the system shown in Figure 4 can be written as

$$(M_I + M_2) \ddot{U} - m_2 \ddot{v} = G - K_I U - F_2^* + F_4^* - M_I \ddot{Y}$$

$$- m_2 \ddot{U} + (M_O + m_2) v = - G - K_O v + F_2^* - F_4^* - M_O \ddot{Y} \quad (24)$$

where the impact elements

$$F_4^* (h_4) = 0 \text{ if } h_4 > 0$$

$$F_2^* (h_2) = 0 \text{ if } h_2 > 0 \quad (25)$$

the fluid mass m_2 is given as

$$m_2 = \frac{\mu \rho c^2}{2} L \left[1 + \frac{1}{3(1-\epsilon_2^2)} \right]$$

and the fluid forces are

$$G = - \frac{\rho c \mu^2}{6} L \frac{\epsilon_2}{(1-\epsilon_2^2)^2} \dot{W}_2^2 - c^*(\epsilon_2) \dot{W}_2 \left| \dot{W}_2 \right| \quad (26)$$

17. It is clear that if the motions U, v are assumed small, then it may be argued that conservative results are obtained by including only the effect of a constant fluid mass $\frac{2}{3} \mu \rho c^4 L$, and neglecting the effect of G. However, if the effect of large motions is incorporated with respect to nominal gap size, then more realistic results can be achieved, since it is easily shown that increases in the fluid effects encompassed in G are larger than the increases in fluid mass.

18. To illustrate the fluid effects, equations (24) and (26) are solved, for a given time history ground motion Y(t), using a modification of the time history computer code presented in Reference 6. Typical geometry and material values are assigned which are representative of a fully loaded fuel rack containing 169 cells simulated by a two degree of freedom dynamic model. Note, however, that such a simple model is only for illustrative purposes; the authors have developed a more realistic rack and fuel assembly group model which uses thirty-two degrees of freedom to accurately simulate potential for rack deformation, impact, and sliding under a realistic 3-D seismic event. For the purpose of illustrating the effects of confined fluid, the following input data is used:

Rack Mass M_O = 9368.8 Kg

Fuel Assembly Mass(169 cells) M_I = 53586.1 Kg

c = .1524 m. : h = 7.9375 mm . ; L = 53.34 m

K_I = 60590.9 N/m. ; K_O = 60590.9 x 10^4 N/m.

f* = 0.025 ; K = .9

ρ = 1019.71 Kg/m^3 x 169 cells = .1723 x 10^6 Kg/m^3

19. To simulate the impact force on the cell walls, non-linear gap elements with stiffness 10 K_O are used. These gap elements become active, when the h_2 or h_4 approach value .01 h.

The seismic acceleration Y(t) used in the simulation is Y(t) = A sin Ω t where

A = .5 g   = 10 Hertz   0 ≤ t ≤ .2 sec

A = 1.0 g   = 5 Hertz   t ≥ .2 sec   (26)

A total event duration of 1.3 sec. is assumed. The following five simulations are performed using the two degree of freedom model:

Case	Remarks
1	Vibration in air; no fluid mass or damping
2	Vibration in fluid; small deflection model - ε_1 = 0 when calculating m_2 and fluid damping effect
3	Vibration in fluid; large deflection model used

for computing fluid masses effect - no fluid damping

4   Same as case 3 except fluid damping included

5   Same as case 4, except f^*, K reduced to 1% of
            (values used in case 4.

Discussion of Results of Simulation Runs

20. The following table summarizes the results obtained from the five simulations. Figures 5 and 7 show typical time histories of the rack spring force. The magnitude of the rack spring force range is a direct measure of the expected rack stress level at the rack base and the subsequent loads transmitted to the pool floor slab through the rack feet (which are not modelled in our simple simulation).

TABLE 1

Summary of Results - Max. Force Range

Case	Rack Spring Force Range ($N \times 10^{-6}$)	Local Impact Force Range from Gap Springs ($N \times 10^{-6}$)	Fluid Damping Force Range ($N \times 10^{-6}$)
1	2.678	12.005	———
2	2.228	9.599	.756
3	1.997	10.555	———
4	1.535	0.	1.503
5	1.766	7.499	4.852

Examination of the maximum force ranges shown in Table 1 produces the anticipated results; namely, the inclusion of fluid damping coupled with large deflection effects significantly reduces the force range in the fuel rack. Comparison of the results of case 4 with case 2 shows a reduction of 31% in the rack force range by the inclusion of large deflection effects in the calculation of fluid mass and fluid damping. The impacts with the cell wall are eliminated, thus eliminating the need for calculation of local impact effects on the rack cell wall. The results of case 3 indicate that at least for this simulated seismic input, the inclusion of only large deflection effects in the fluid virtual mass and the complete neglect of fluid damping serves to reduce the force range in the rack. The local stress range in the rack cell wall is increased in this case however. The authors hesitate to draw any lasting conclusions from the case 3 results since a change in input seismic frequence content may very well reverse the conclusions inferred from this data.

21. The results obtained in case 5 merit some further elaboration. The reduction in fluid damping to 1% of the values used in case 4 is an attempt to simulate the possible damping effect of unchannelled fuel assemblies. It is clear that the damping and virtual mass effects from an unchannelled fuel assembly should be substantially less since the confined fluid has more unobstructed area in which to flow as the fuel assembly moves relative to the cell wall. In addition, there are substantial differences in the flow-field which should be considered in any analysis of unchannelled fuel. Nevertheless, case 5 may give some indication of what might be expected if only unchannelled fuel assemblies are in the rack. Table 1 shows that the rack force range certainly increases over the results obtained in case 4; the rack force level is still substantially less than the results obtained for case 2. Local impact with the rack cell wall occurs during the event although the impact range is less than that of case 2. A somewhat surprising results, on first reading, is obtained for the maximum fluid damping force range. Since the damping coefficients have been reduced, one might expect that the damping force range should also be reduced. However, we recall that the damping force is of the form

$$F_d \sim C(\varepsilon) \, \dot{W} \left| \dot{W} \right| \tag{27}$$

$\dot{W}$ is maximum when $\varepsilon \sim 0$, and goes to zero as the gap closes. $C(\varepsilon)$ achieves its largest value when the gap closes, and is relatively small when $\varepsilon \sim 0$. Examination of the detailed numerical output from the simulations show that the damping force exhibits a sharper and higher peak in case 5, compared to case 4, but the energy dissipation due to the fluid damping is higher in case 4. The increased dissipation in case 4 precludes $C(\varepsilon)$ from growing too large since the gap never becomes too small. The effect of fluid damping on the rack spring force range is measured by the dissipation level during the event, rather than the peak value of the fluid damping force. Thus, the expected result that a decrease in the effective fluid friction coefficient results in increased rack force level is obtained.

22. Examination of the detailed time history of rack force level shows that in air the rack essentially vibrates at its natural frequency of 41 Hertz with amplitudes modified by the local impact forces. Although not shown here in the results, during the 1.3 second time of the event, vibration in air results in a total of twenty-two impacts with the outer cell walls. With the additional of fluid mass, the graphs show that the rack essentially vibrates at the forcing frequency of either 10 or 5 Hertz.

The addition of fluid mass effects in cases 2-5 reduces the number of impacts to a total of three during the time span of the event.

CONCLUSIONS

23. It has been demonstrated that in high density fuel racks containing channelled fuel assemblies, large displacement effects coupled with the inclusion of fluid damping results in a significant decrease in rack force range and possibly the complete elimination of local impacts between rack cell and fuel assembly. It has also been shown that an approximate analysis of the large displacement effect is easily implemented into a time history lumped mass analysis. In a 3-D motion cross coupling effects between the two on-plane motions will occur in the inertial terms due to

the large displacements; although not carried out in detail herein, similar cross coupling in the fluid damping terms is expected.

24. Experimental work is currently planned to verify the analysis presented here. Once the analysis has been matched with experiment, for both channelled and unchannelled fuel, the accurate inclusion of fluid damping effects should become an accepted feature of the 3-D dynamic analysis of high density fuel storage racks.

REFERENCES

1. Sharp G R and Wenzel W A. "Hydrodynamic Mass Matrix for a Multibodies System", Journal of Engineering for Industry, Trans. of the ASME, pp. 611-618, May 1974.

2. Fritz R J. "Effect of Liquids on the Dynamic Motions of Immersed Solids", Journal of Engineering for Industry, Trans. of the ASME, February 1972, pp. 167-173.

3. Stokey W F and Scavuzzo R J. "Normal Mode Solution of Fluid-Coupled Concentric Cylindrical Vessels", Trans. of the ASME, Vol. 100, Journal of Pressure Vessel Technology, pp. 350-353, November 1978.

4. Dong R G. "Size Effect in Damping Caused by Water Submersion", AICE, Journal of the Structural Division, May 1979, pp. 847-857.

5. Li W H and Lam S H. Principles of Fluid Mechanics, Addison Wesley, 1964, pp. 273-278.

6. Levy S and Wilkinson J P D. The Component Element Method in Dynamics, McGraw Hill, 1976, Chapter 3.
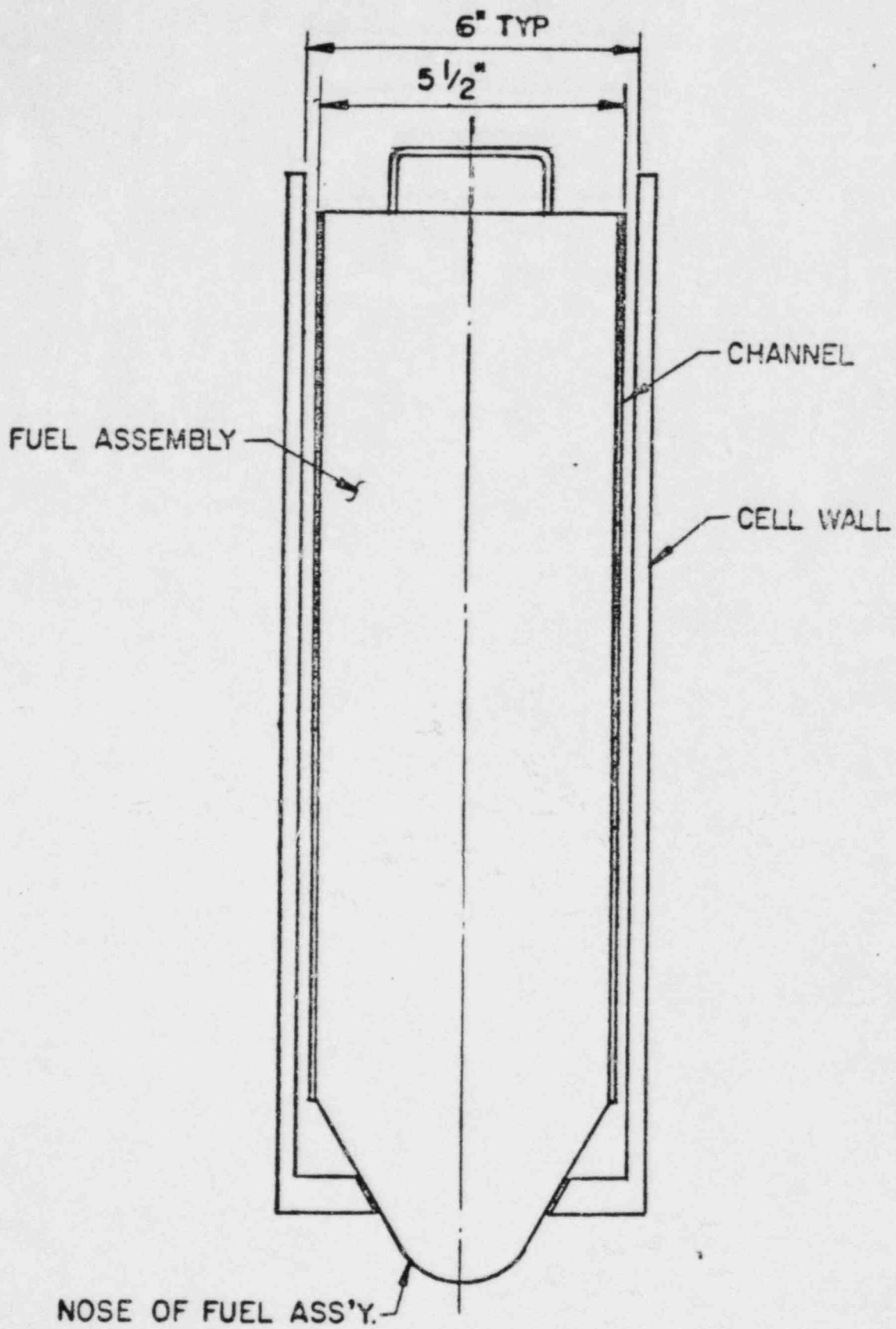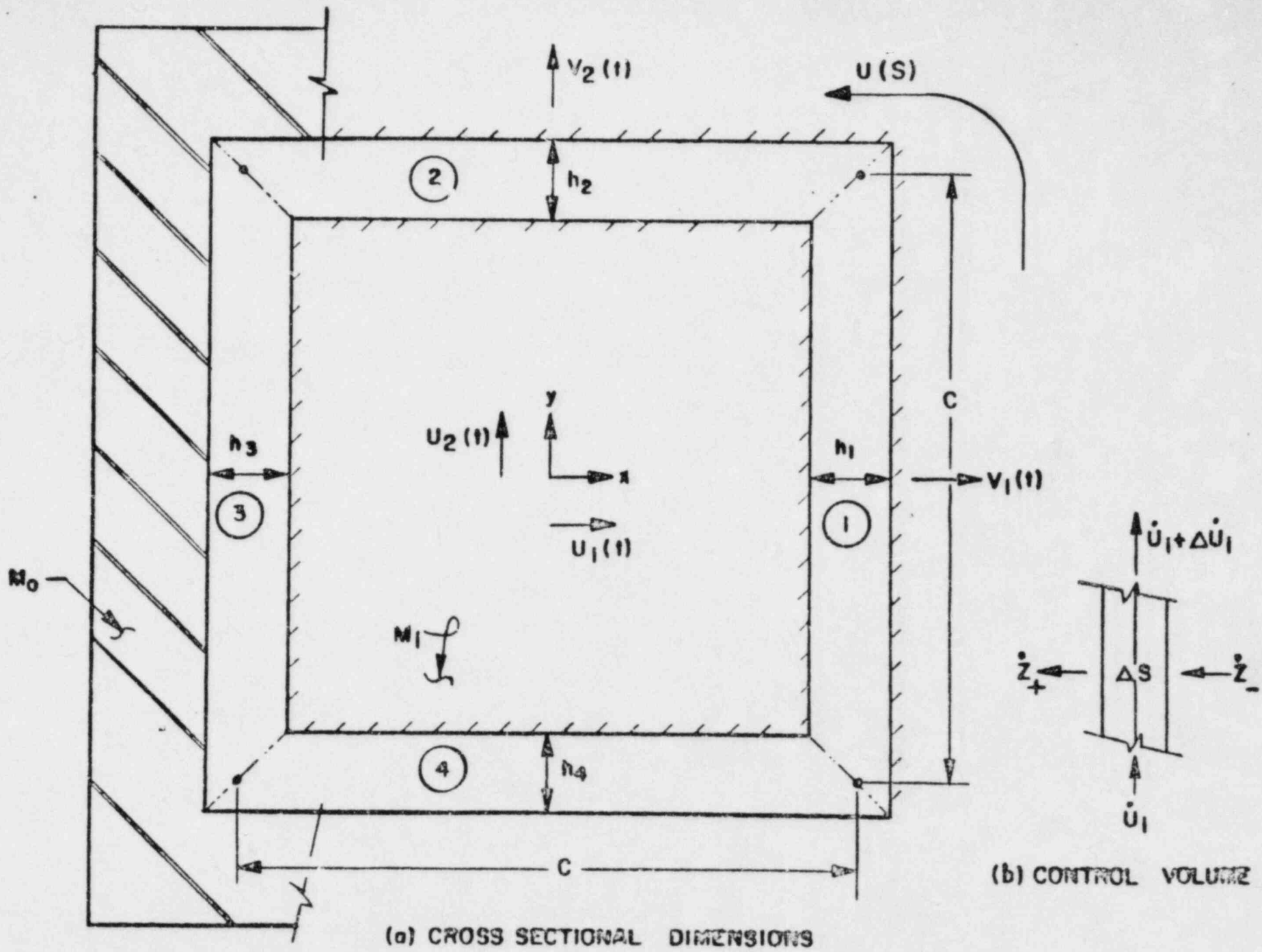
6" TYP

5 1/2"

CHANNEL

FUEL ASSEMBLY

CELL WALL

NOSE OF FUEL ASS'Y.

FIG.1; TYP. BWR FUEL ASSEMBLY IN CELLULAR CONTAINER.

827

(a) CROSS SECTIONAL DIMENSIONS

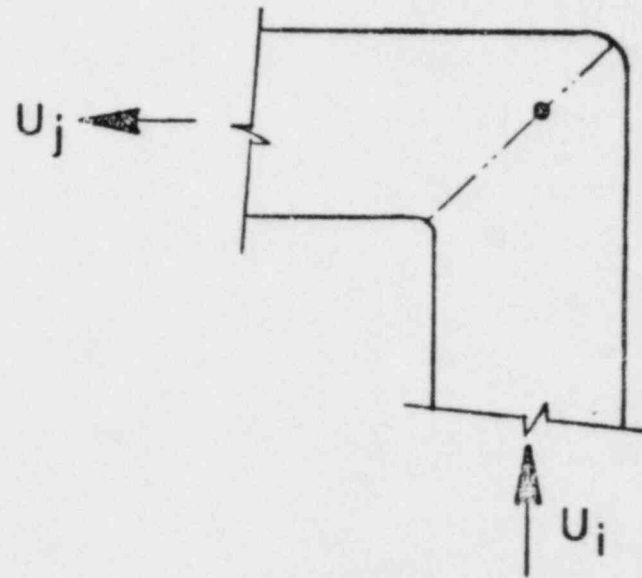(b) CONTROL VOLUME

FIGURE 2

FIGURE 2
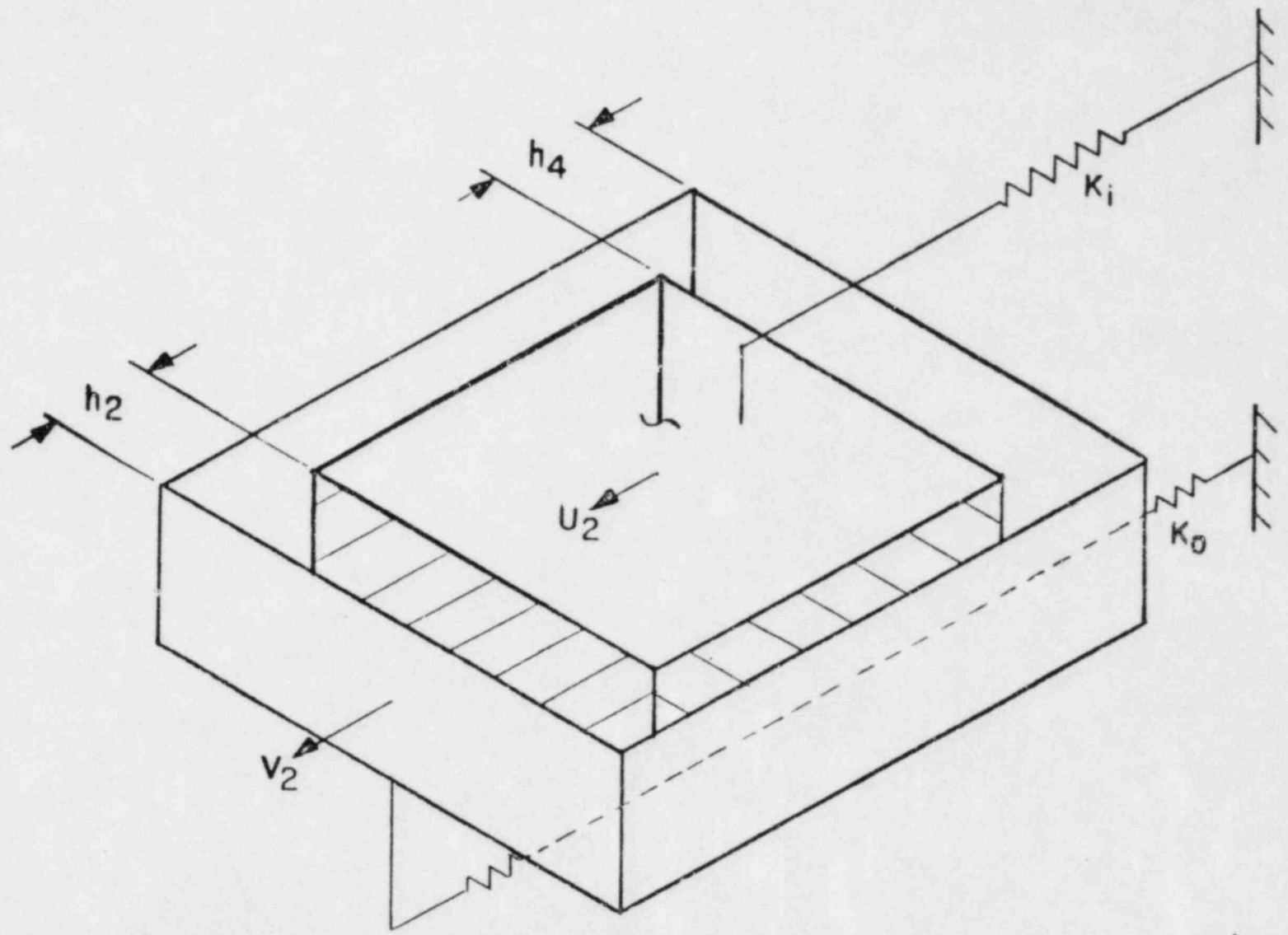

FIG. 3 ; CONTINUITY AT A CORNER.
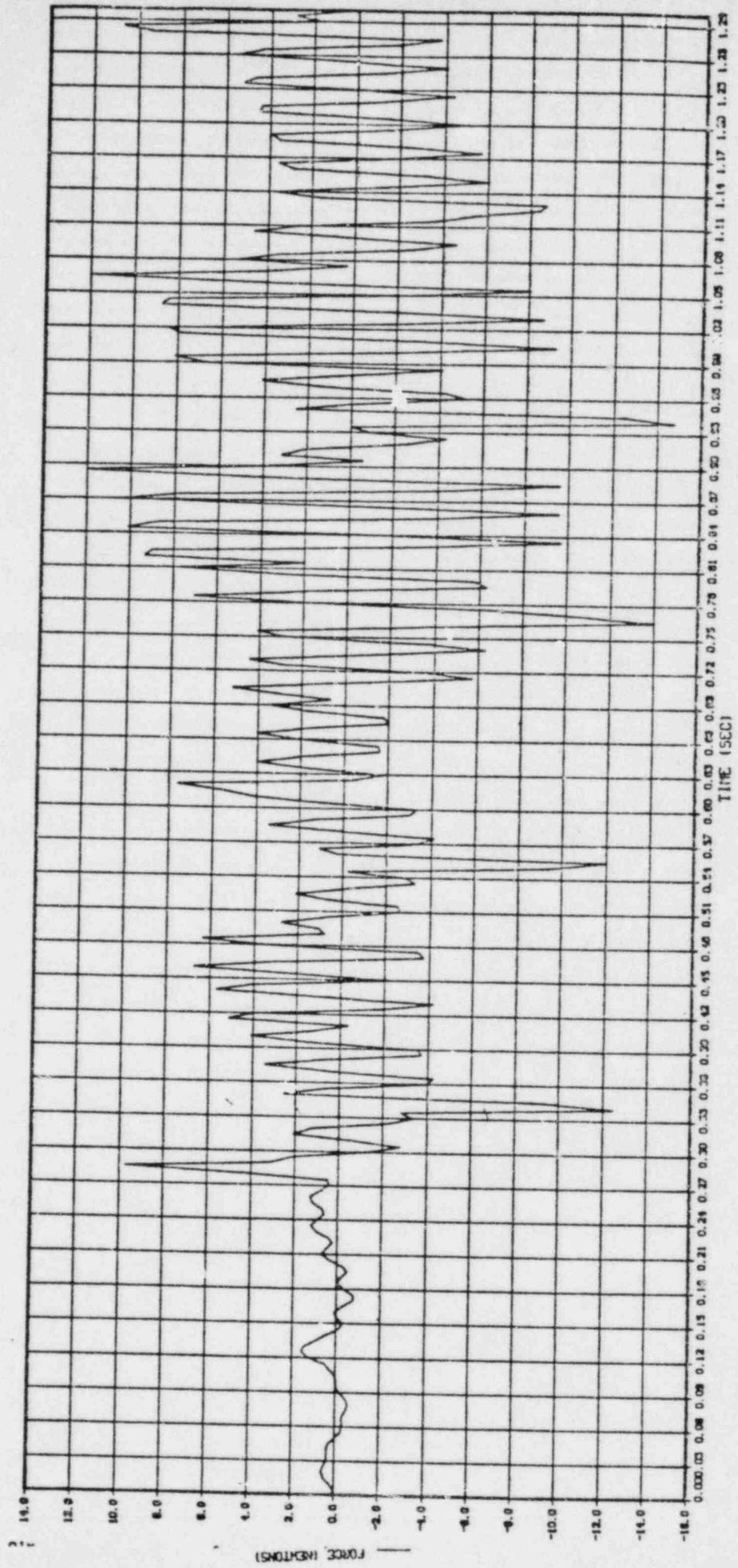
FIGURE 4; DYNAMIC MODEL.

FIG. 5; CASE 1 NO FLUID

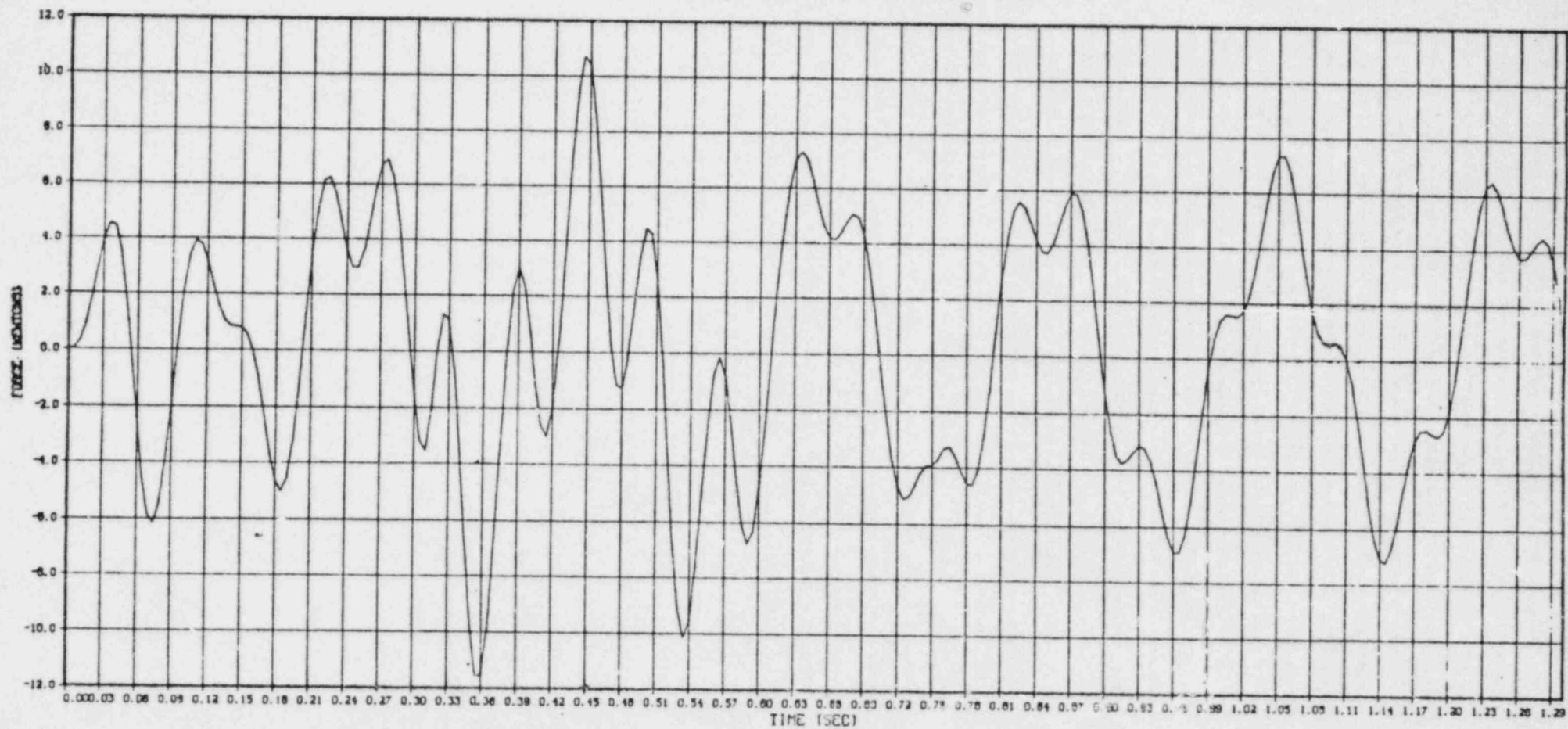FIG. 6; CASE 2 FLUID MASS AND
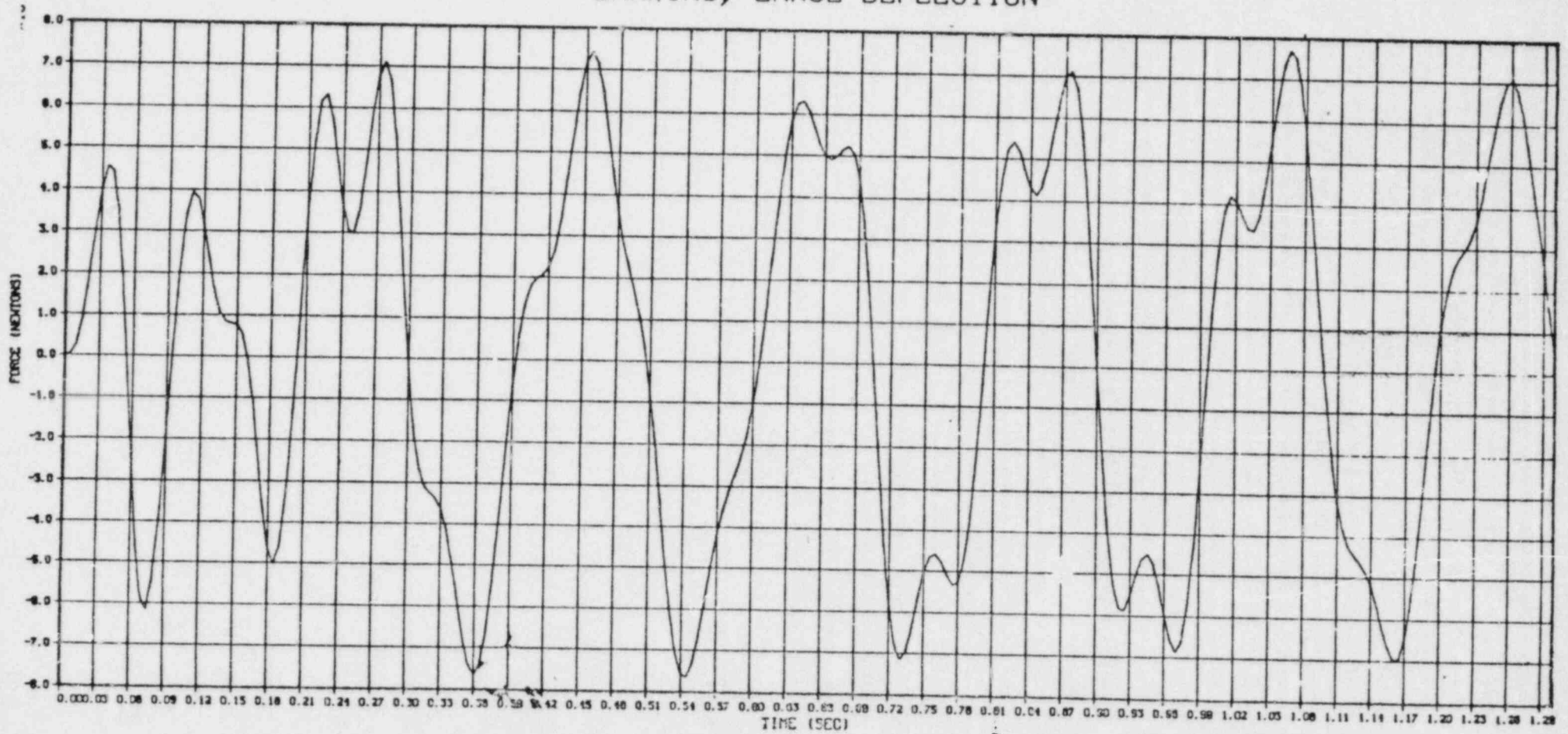DAMPING, SMALL DEFLECTION

FIG. 7; CASE 4 FLUID MASS AND
DAMPING, LARGE DEFLECTION

PRESENTATION AND DISCUSSION

In presenting the paper Dr. SOLER said that it dealt with work arising from a seismic analysis and qualification of high density spent fuel storage racks. He defined the problem and gave an outline of the model adopted with the assumption of no axial vibration. He discussed the derivation of fluid velocity field and the calculation of fluid kinetic energy and damping forces. He gave a numerical example and discussed the results.

Dr. J.D. DUTHIE (UKAEA) noted that the force transmitted to the support was reduced by the inclusion of large added mass terms and asked why that was. Dr. SOLER discussed this in the terms of the way the damping built up and the analysis which included all the large deflection effects as compared with the case which only included the small mass effects. The force in the rack spring was 30% less for the former. Mr. DUTHIE thought they would be about the same. He then asked if Dr. SOLER had any feel for how short the length of the axial contact needs to be before the assumption of no axial fluid velocity breaks down. He thought this would reduce the very large values of added mass. Dr. SOLER said he would expect that the inclusion of axial terms would reduce the 30% result to maybe 20% because the flow would split i.e. the present results probably gave an upper boundary.

Dr. D.E. HOBSON (CEGB) said that he would expect that at the ends of the storage racks the high fluid pressures predicted would not be realised due to axial movement and this would induce a pressure distribution which was very non-uniform in the axial direction. This would introduce close distortion of the element, bending and axial motion. Dr. SOLER agreed.

To appear, in

Nuclear Engineering and Design,

American Nuclear Society (c.1984)

Seismic Response of Free Standing Fuel Rack Construction to 3-D Floor Motion

by

Alan I. Soler
Professor of Mechanical Engineering and Applied Science
University of Pennsylvania
Philadelphia, Pennsylvania

and

Krishna P. Singh
Vice President of Engineering
Joseph Oat Corporation
Camden, New Jersey

Seismic analysis of free standing submerged racks is complicated by the presence of water and structural non-linearities such as fuel assembly cell impact and floor interface friction. A direct time integration technique has been proposed to analyze this class of structures. Application of the time integration technique on a fourteen degree of freedom lumped mass model of the rack reveals some heretofore unpublished quirks in the structure's behavior. The method of analysis is utilized to compare the seismic response of some representative rack designs. Results show wide differences in the structural response, depending on the fabrication details of racks.

Introduction:

Subsequent to the U.S. government announcement of indefinite suspension of spent fuel reprocessing in 1977, the nuclear power industry has scrambled to increase its capacity for on-site storage. The storage pools in most of the commercial reactors were initially designed to store 1-1/3 core worth of spent fuel. The storage rack modules, built for storing the spent fuel in the pool, were typically of open lattice construction. The racks were anchored to the pool floor, and were frequently braced to the side walls of the pool and to each other. Wide pitch (center-to-center spacing) between the storage locations ensured subcriticality of the fuel array. Ostensibly, the most viable and cost effective procedure to increase fuel pool storage capacity lay in replacing these rack modules with the so-called high density racks. The latest version of high density racks consists of cellular storage locations arranged in a tight pitch with neutron absorber materials interposed between the cells to maintain nuclear subcriticality. Matching of the new "high density rack supports" with the original floor anchor locations is usually quite cumbersome, if not impossible. Moreover, it is desirable to minimize the in-pool installation time for personnel radiation safety. These considerations, among others, prompted the evolution of the free standing high density racks storage concept. Increasingly, the new generation high density racks are being designed for free standing installation. The structural analysis of such racks under postulated floor motions, referred to as Safe Shutdown and Operating Basis earthquakes in the lexicon of the nuclear power industry, is the subject of this paper. Representative of other work in this area of interest is the rather qualitative paper by Habedank and co-authors [1].

1

A free standing rack module is a highly non-linear structure. During a seismic event the fuel assemblies can "rattle" inside their storage locations, and the module itself may slide on the pool floor. Furthermore, the rack may lift off at one or more support feet locations causing impact between pool floor and the rack support structure. Exigency of the market place calls for economies in design and construction; however, reduction in the rack structural strength can only be made after an exhaustive analysis of the resultant non-linear effects. In this paper we present a technique which can be utilized to make such an analysis.

To illustrate the procedure, we consider two types of rack construction; one in which the storage cells are attached to each other along their long edges in a certain pattern (honey-comb construction) and another in which the connection between the cells is made only at the top and bottom (end connected tube construction). The latter construction involves only a fraction of the welding of the former, and therefore is a far more economical design. From a safety standpoint, the overriding concern relates to the increase in the rack stress levels and rigid body displacements as the inter-cell longitudinal welds are eliminated. It is necessary to develop a methodology to address such concerns during the initial design and licensing effort. This paper is intended to provide such a tool.

A storage rack is a structure submerged in water which greatly complicates its motion. Proper simulation of rack dynamics requires consideration of hydraulic coupling and virtual mass effects. Such effects are included in this analysis using simplified models. Since our object herein is to establish a tool for comparison purposes only, we propose a fourteen degrees-of-freedom model to simulate rack behavior. A more comprehensive model has been employed by the authors in analyzing racks for individual plants [2]. It is important to emphasize that what we are demonstrating here is a simpler version of what would be required to qualify an actual unit; however, the

methodology employed to develop the model is essentially the same.

Comparison of different rack geometries on the basis of their structural response is affected by three major variables; (i) the acceleration time history, which varies from plant to plant, (ii) the fraction of module storage locations occupied, (iii) and the limiting static and dynamic coefficients of friction at the rack and pool floor interface. In order to draw tenable conclusions, analyses are performed using three arbitrary sets of earthquake time histories. Two conditions of rack loading (all or half of the locations occupied), and two values of the coefficients of friction are also considered. In all a total of six cases are utilized to infer characteristics of the rack structural behavior.

The three orthogonal seismic excitations are applied coincidentally. The results reveal some striking peculiarities of the rack three-D structural response. The marked increase in the rack stress levels and displacements predicted by this study as the design is varied from the "honey-comb" to "end connected" construction highlights the problem areas of the latter design. Perhaps more important, beyond the numerical results presented here, the analysis suggests a methodical technique to evaluate candidate designs for a particular application.

THEORY

We consider a system governed by absolute generalized coordinates $p_i(t)$, $i=1,2...N_z$. All internal forces contributing to system deformation are associated with generalized extensions $\delta_j(p_i)$. Internal force elements F_j may be non-linear functions of the generalized deformations $p_i(t)$ such as gap or friction elements. Lagrange's equations, written in terms of generalized forces $Q_i(t)$, and

3

generalized external forces $G_i(t)$ are

$$\frac{d}{dt} \left(\frac{\partial T}{\partial \dot{p}_i} \right) - \frac{\partial T}{\partial p_i} = Q_i(t) + G_i(t) \qquad (1)$$
$$i = 1, 2 \ldots N_z$$

Since all of the $p_i(t)$ are independent, it is easily demonstrated that

$$Q_i(t) = \sum_{k=1}^{N_f} F_k \frac{\partial \dot{\delta}_k}{\partial \dot{p}_i} = \sum_{k=1}^{N_f} F_k B_{ik} \qquad (2)$$

where the dot (·) indicates time derivative and B_{ik} are called coupling coefficients [1]. B_{ik} relate the generalized velocities $\dot{p}_i(t)$ and the generalized extension rates $\delta_K(t)$. The system kinetic energy T is written as

$$T = \frac{1}{2} \sum_{i=1}^{N_z} \sum_{j=1}^{N_z} M_{ij} \dot{p}_i \dot{p}_j \qquad (3)$$

For a geometrically linear system (equilibrium equations based on the undeformed configuration), the generalized masses M_{ij} are independent of coordinates p_k. Using eqs. (2) and (3) in eq. (1) yields the system equations of motion in the form

$$[M]\{\ddot{p}\} = [B]\{F\} + \{G\} \qquad (4)$$

where $[M]$ is of order $N_z \times N_z$; $[B]$, the coupling coefficients matrix, is of order $N_z \times N_f$, $\{p\}$, $\{G\}$ are column matrices containing N_z rows, and $\{F\}$ is a column matrix containing N_f rows. A set of inertially decoupled equations evolved from eq. (5), is

4

$$\{p\} = [M]^{-1}[B]\{F\} + [M]^{-1}\{G\} \tag{5}$$

Equations (5) are solvable by direct integration techniques using a time history computer code described in Ref. 3 (p. 336).

FUEL RACK MODEL

The following items should be considered in the development of any fuel rack - fuel assembly dynamic model:

1. Modelling of the rack structure

The rack structure may be modelled by elastic beam elements as long as appropriate cross section properties can be derived and as long as shear deformation and rotatory inertia effects are included. In specific design applications, the authors have used four beam elements and five nodal points to describe the rack structure. In this paper, since the emphasis is on a comparison of two different rack geometries, we have adopted a simpler model for the rack structure involving only a single beam element. This simplification helps to focus attention on the main differences between the two rack configurations studied; namely, the significant difference in the shear resistance.

2. Modelling of the fuel assemblies

Each fuel assembly should be treated as an individual distributed mass elastic element. In the actual fuel rack, an element may be located anywhere in the x-y plane and will impact with the fuel rack surrounding metal at one or more vertical locations. An assemblage of fuel assemblies will certainly not move in phase during a seismic event. For the purposes of evolving a conservative model, we have assumed that all of the fuel assemblies move as a unit; thus, the impacts with the fuel

rack are magnified leading to higher stress and load levels. In a detailed model where the rack is simulated by five nodal points, impacts between fuel rack and fuel assemblies may occur at different levels; in the simpler model used herein for comparison purposes, we assume that impact between fuel rack and fuel assemblies occurs only at the top of the rack, and that 50% of the fuel assembly mass is involved in any impact with the rack. We emphasize that in any real design study, the possibility of impacts at various heights should be included in the model. For this illustrative comparison, we feel that the salient features of the behavior of each rack type will be correctly demonstrated with the simpler model.

Figures 1 and 2 show the model considered in this paper. The fuel rack metal structure is a single beam element whose end points have a general six degree of freedom motion. The ensemble of fuel assemblies are conservatively assumed to move in phase under seismic excitation, and their effect on the fuel rack is considered to have the potential of 50% of the effective mass impacting the rack at the uppermost point. The offset of the lumped mass from the rack beam centerline enables simulation of a partially filled rack with induced torsional moments. The fuel rack base is a rigid plate, supported at the four corners by rigid supports that may slide or lift off the pool floor. The pool floor is excited by a known ground acceleration in three orthogonal directions.

Fluid coupling between rack cell walls and the ensemble of fuel assemblies is simulated by introducing appropriate inertial coupling terms into the system kinetic energy. Similar inertial coupling is introduced to account for fluid structure effects between adjacent racks. Fluid damping effects are neglected in this study. As shown in Figure 2, potential impacts between the

6

rack beam and the lumped mass representing the fuel assemblies are accounted for by inclusion of appropriate gap elements. The fluid inertial coupling terms are based on nominal clearances in this investigation; however, it has been shown [4] that inclusion of large deformation effects near the impact points may considerably affect the results. Herein, we do not include the effects of gap closure on the fluid inertia terms since there is some preliminary evidence [4] that neglect of the effects is conservative.

In computing kinetic energy contributions from the rack, we use appropriate consistent mass matrices. Therefore, the contribution to the system kinetic energy due to the rack, T_1, is given by

$$2T_1 = \{\dot{p}_3, \dot{p}_{14}\}^T [M_E] \left\{ \begin{matrix} \dot{p}_3 \\ \dot{p}_{14} \end{matrix} \right\} + \{\dot{p}_6, \dot{p}_{13}\}^T [M_T] \left\{ \begin{matrix} \dot{p}_6 \\ \dot{p}_{13} \end{matrix} \right\}$$

$$+ \{\dot{p}_1, \dot{p}_7, \dot{p}_5, \dot{p}_{12}\}^T [M_B] \left\{ \begin{matrix} \dot{p}_1 \\ \dot{p}_7 \\ \dot{p}_5 \\ \dot{p}_{12} \end{matrix} \right\} \qquad (6)$$

$$+ \{\dot{p}_2, \dot{p}_9, -\dot{p}_4, -\dot{p}_{11}\}^T [M_B] \left\{ \begin{matrix} \dot{p}_2 \\ \dot{p}_9 \\ -\dot{p}_4 \\ -\dot{p}_{11} \end{matrix} \right\}$$

where $[M_E]$, $[M_T]$ and $[M_B]$ are the appropriate mass matrices for extensional, torsional and flexural motions.

7

If A, I_p are the rack cross section effective metal area and polar moment of inertia, respectively, then

$$[M_E] = \frac{\rho_v^* AH}{3} \begin{bmatrix} 1 & 1/2 \\ 1/2 & 1 \end{bmatrix} \; ; \; [M_T] = \frac{\rho I_p^* H}{3} \begin{bmatrix} 1 & 1/2 \\ 1/2 & 1 \end{bmatrix} \quad (7)$$

$$[M_B] = \rho^* AH \begin{bmatrix} \frac{13}{35} & \frac{9}{70} & \frac{11\,H}{210} & -\frac{13H}{420} \\[2mm] \frac{9}{70} & \frac{13}{35} & \frac{13H}{420} & -\frac{11\,H}{210} \\[2mm] \frac{11H}{210} & \frac{13H}{420} & \frac{H^2}{105} & -\frac{H^2}{140} \\[2mm] \frac{-13H}{420} & \frac{-11H}{210} & \frac{-H^2}{140} & \frac{H^2}{105} \end{bmatrix} \quad (8)$$

ρ^* and ρ_v^* are effective mass densities accounting for fluid effects. The contribution to the system kinetic energy due to the rack base is

$$2T_2 = m_{b_1}\dot{p}_1^2 + m_{b_2}\dot{p}_2^2 + m_{b_3}\dot{p}_3^2 + I_x\dot{p}_4^2 + I_y\dot{p}_5^2 + I_z\dot{p}_6^2 \quad (9)$$

where m_{bi}, I_x, I_y, I_z are the effective mass, and mass moments of inertia of the base, including fluid mass effects.

The contribution to system kinetic energy due to fluid coupling between fuel rack and fuel assemblies is expressed by the 2-D model given in Reference [5]. The necessity for accounting for 3-D fluid structure interaction is a question that merits future study. Using the 2-D approximation, we obtain for the kinetic energy due to rack-assembly interaction,

8

$$2T_3 = A_{22}(\dot{p}_7{}^2 + \dot{p}_9{}^2) + A_{11}(\dot{p}_8{}^2 + \dot{p}_{10}{}^2) + 2A_{12}(\dot{p}_7\dot{p}_8 + \dot{p}_9\dot{p}_{10}) \quad (10)$$

Similarly, the kinetic energy due to fluid coupling between a fuel rack and adjacent structure is given as

$$2T_4 = B_{11}^{(x)}\dot{p}_1{}^2 + B_{11}^{(y)}\dot{p}_2{}^2 + B_{11}^{(x)}\dot{p}_7{}^2 + B_{11}^{(y)}\dot{p}_9{}^2$$

$$+ 2B_{12}^{(x)}\dot{p}_1\dot{U}_1 + 2B_{12}^{(y)}\dot{p}_2\dot{U}_2 + 2B_{12}^{(x)}\dot{p}_7\dot{U}_1 + 2B_{12}^{(y)}\dot{p}_9\dot{U}_2 \quad (11)$$

$$+ 0\ (\dot{U}_1{}^2, \dot{U}_2{}^2)$$

where U_i (i=1,2,3) are specified pool floor seismic motions.

Finally, the contribution to the system kinetic energy due to the mass of the fuel assembly group is written as

$$2T_5 = \lambda M\ (\dot{p}_8{}^2 + \dot{p}_{10}{}^2) + M(\dot{p}_3 + Y_B\ \dot{p}_4 - X_B\ \dot{p}_5)^2$$

$$+ (1-\lambda)M\ \left[(\dot{p}_1 - Y_B\dot{p}_6)^2 + (\dot{p}_2 + X_B\dot{p}_6)^2\right] \quad (12)$$

M is the total fuel assembly mass and λ is the mass fraction assumed acting at the top of the rack in the horizontal plane. We have assumed that vertical movement of the fuel assemblies is equal to the vertical movement of the rack base at fuel assembly centroid location, and that the fuel assembly mass fraction $(1-\lambda)$ M moves with the base in the X-Y plane. In the study herein, we have arbitrarily set $\lambda = .5$ which implies that 50% of the fuel assembly mass is involved in the impact process and the impacts

9

all occur at the top of the rack. If more conservatism is desired λ may be increased. It would be far better to include more degrees of freedom and allow for the possibility of impacts below the top level, however, than to attempt to determine a proper value for λ. For the purposes of the comparison simulation here, it is felt that the value of λ used will not negate any conclusion developed as long as λ is sufficient to induce significant impacts between rack and assemblies. Equations (6)-(12) establish the system mass matrix $[M]$ in equation (4) for the 14x14 model considered herein. We introduce displacement coordinates $q_i(t)$, relative to ground, defined as follows:

$$
\begin{aligned}
P_i &= q_i + U_1(t) & ; && i &= 1,7,8 \\
P_i &= q_i + U_2(t) & ; && i &= 2,9,10 \\
P_i &= q_i + U_3(t) & ; && i &= 3,14 \\
P_i &= q_i & ; && i &= 4,5,6,11,12,13
\end{aligned} \tag{13}
$$

The governing equations may be represented as follows:

$$
\sum_{j=1}^{14} M_{ij} q_j = Q_i(t) + G_i(t) - \left[\alpha_{i1} U_1 + \alpha_{i2} U_2 + \alpha_{i3} U_3 \right] \tag{14}
$$

$$
i = 1,2,\ldots 14
$$

In what follows, we discuss briefly the computation of some of contributions to the elements of the set of equations [14].

FLUID ADDED MASS EFFECTS

Consider a typical cell with an internal fuel assembly shown in Fig. 3. Assuming that the assembly and the cell are vibrating, it is shown by Fritz [5] that the constant coefficients A_{ij} of

10

equation (10) are given as

$$A_{11} = M_H \; ; \; A_{12} = - (M_1 + M_H) \; ; \; A_{22} = M_1 + M_H \tag{15}$$

where M_1 = fluid mass displaced by fuel assembly

M_H = hydrodynamic mass

We use the Fritz model for concentric cylinders employing equivalent radii R_1, R_2 defined as

$$R_1 = a^*/\sqrt{\pi} \qquad R_2 = b^*/\sqrt{\pi} \tag{16}$$

a^* is the side length of the square fuel assembly and $b^* > a^*$ is the inside dimension of a typical square cell; i.e. the nominal clearance between assembly and cell is $(b^*-a^*)/2$.

For a rack of height H, assuming all assemblies move in phase, we obtain

$$M_1 = \pi \rho_w H R_1^{\,2} f_a \tag{17}$$

where f_a is the number of cells containing spent fuel assemblies. If the nominal gap g is defined as $g = (b^*-a^*)/2$, then [5] suggests that the hydrodynamic mass is

$$M_H = \frac{R_1}{g} M_1/(1 + 12 \, R_2^{\,2}/H^2) \tag{18}$$

The fluid mass that would fill the cell volume in the absence of the fuel assembly is denoted by M_2 in [5]; the effect of this virtual fluid mass is incorporated directly in eq. (8) by defining an effective ρ^*.

The effect of fluid inside of the rack structure has been accounted for in the kinetic energy term $T_3(A_{ij})$. We now consider the effect of the fluid outside of the rack (say between the rack being studied and adjacent structures). We consider Figure 4 which shows a vibrating vertical wall of width W and height H. Following case 13 of Reference [5], we assume the hydrodynamic mass term as

$$M_H = \frac{\rho_w W^3 H}{12 g_0 \psi} \quad ; \quad \psi = 1 + \frac{W}{H} \tag{19}$$

Then, in the fourteen degree of freedom simulation model, the coefficients B_{11}, B_{12} at each level are given as

$$B_{11} = M_H/2 \quad ; \quad B_{12} = - (M_H + \rho_w H W t_p)/2 \tag{20}$$

with W being the value appropriate for X or Y motion.

The above discussion is concerned with fluid coupling effects induced by horizontal vibrations. To account for fluid effects in vertical vibrations, we simply define an effective mass density for the base plate using case 6 of Reference 5 and add it to the base plate metal mass. The total effective mass density is then used in the computation of m_{b_3}, I_x, I_y for the base plate. The effect of virtual fluid movements on the rack is simulated by defining an effective mass density ρ_v^* in the matrix $[M_E]$ in equation (8). ρ_v^* is computed by adding to the rack metal mass, a mass equal to the mass of fluid displaced by the rack.

INTERNAL FORCES

The internal force elements representing system elasticity, disappative friction and impact effects are simulated by using

12

standard spring, friction and gap elements described in Reference 3. The model shown in Figure 1 contains 6 elastic springs to model two bending planes, extension, and torsion of the rack beam. The model contains four gap elements modelling contact between the fuel assembly lumped mass and the top of the rack. The model uses four gap elements aligned in the vertical direction and located at the x,y coordinates of the base plate supports to simulate the support behavior in the vertical direction and has sixteen friction elements to simulate support leg flexibility and the sliding potential of the supports. Finally, eight rotational frictional elements at the base supports are used to simulate resisting moments due to floor-structure interaction. Full details of the behavior of these elements and the development of their associated coupling coefficients are found in [3]; herein, we simply specify the spring rates associated with each of the elements.

<u>RACK ELASTICITY</u> (6 Elements)

$$K_{TORSION} = GIp/H$$

$$K_{EXTENSION} = EA/H$$

$$\text{(21)}$$

$$K_{SHEAR} = \frac{12\ E\ I}{H^3(1+\phi)} \quad ; \quad \phi = \frac{12\ E\ I\ \alpha}{G\ A\ H^2}$$

$$K_{BENDING} = \frac{E\ I}{H}$$

The coefficient α represents the effect of shear deformation, and I is the area moment of inertia of the cross section associated with beam bending. Note that one shear and bending spring pair is needed for each plane of bending.

13

IMPACT SPRING RATE (4 Gap Elements)

The potential impact between fuel assembly mass and fuel rack is simulated by incorporation of a spring-gap combination. Each impact element acts in compression only with spring constant given as

$$K_I = f_a 64\pi D/a^2 \quad ; \quad D = Et^3/12(1-\nu^2) \tag{22}$$

K_I is determined by assuming that the impact is simulated by a uniform pressure acting over a circular section of cell wall of radius a and thickness t. The radius a is taken as $b^*/\sqrt{\pi}$ where b^* is the inside dimension of an individual cell and f_a is the number of cells containing fuel assemblies.

SUPPORT LEG SPRING RATE (4 Gap Elements)

The effect of support legs at each corner of the fuel rack base is simulated by four compression only gap elements to permit lift off of any or all supports. The local spring rate K_S for a support of height h is

$$\frac{1}{K_S} = \frac{1}{K_F} + \frac{1}{K_{LF}} + \frac{1}{K_{LR}} \tag{23}$$

where $K_F = E \, A_S/h$; A_S = support leg cross section area.

and $K_{LF} = 1.05 \, E_c B/(1-\nu^2)$; $K_{LR} = 1.05 \, \eta \, E \, B/(1-\nu^2)$ (24)

K_{LF} represents the local elasticity of the pool floor with E_c being the Young's modulus of concrete and B being the width of

14

the support leg pad [3]. K_{LR} represents the local elasticity of the rack just above the support leg; the coefficient η is taken arbitrarily as equal to the ratio of the metal area of single cell to included area of single cell.

FLOOR ROTATIONAL AND FRICTION ELEMENTS

The effect of local floor elasticity on rocking motion (support leg bending) is represented by rotational springs with spring rate ([3] p. 293).

$$K_H = E_c B^3/6(1-v^2) \tag{25}$$

These rotational springs are moment limited since if edging of the pad occurs, no further moment can be resisted.

Associated with each support leg compression element spring are two orthogonal friction elements located in the plane $Z = -h$ (See Figure 1). The friction element local spring rate is assumed as the spring constant of a support leg when considered as a guided cantilever beam of length h under an end load P. Therefore, from [6], assuming that the support has area moment of inertia I_s when considered as a beam,

$$K_f = \frac{12 E I_s}{h^3} \quad \frac{1}{(1+\psi)} \quad ; \quad \psi = 8.52 \frac{I_s}{A_s h^2} - 4.157 \left(\frac{I_s}{A_s h^2}\right)^{3/2} \tag{26}$$

APPLICATION TO TYPICAL UNITS

Figures 3 and 5 show a cross section through a level of the rack structure of two practical rack constructions. The first is a fully connected honeycomb construction (HCC) which is considered as a beamlike structure with cross section dimensions

15

b and a, having certain area and inertia properties; the second is an end connected tube construction (ETC) which has no shear transfer capability between tubes except at top and bottom of the rack. For the HCC rack, equation (21) can be used directly to model rack elasticity since the entire cross section is capable of beamlike shear transfer; we need only examine the cross section details to derive expressions for A, I, I_p. For the ETC construction, however, since no shear transfer between cells can occur, we must undertake additional analysis in order to arrive at the proper spring rates for Equation (21).

Figure 6 shows a free body of the rigid ring connecting all of the tube like cells at z=H and constrains them to move as a unit. If there are J cells at level i, then equilibrium requires that for a 2-D motion.

$$M^* = \sum_{j=1}^{J} \left[\sum_i (M_{ij} + y_i N_{ij}) \right]$$

(27)

$$V^* = - \sum_{j=1}^{J} \left[\sum_i^i V_{ij} \right] \quad ; \quad N^* = \sum_{j=1}^{J} \sum_i N_{ij}$$

Castigliano's Theorem for the ith tube yields (assuming a fixed base)

$$V_{ij} = - \frac{12 \, E \, I}{H^3} \, W^* - \frac{6 \, E \, I}{H^2} \, \theta^*$$

(28)

$$M_{ij} = + \frac{6 \, E \, I}{H^2} \, W^* + \frac{4 \, E \, I}{H} \, \theta^*$$

16

Also, bearing in mind the constraint of the end closure, we have,

$$N_{ij} = \frac{E\,A}{H}\left(U^* + y_i\,\theta^*\right) \tag{29}$$

In equations (28), (29), A, I refers to the properties of the individual cell, and we have neglected shear effects in the bending of the individual cells. Using eqs. (28), (29), in eq. (27) yields, for the case of n total cells in the unit,

$$M^* = + \frac{6\,E\,(n\,I)\,W^*}{H^2} + \frac{4\,E}{H}\left\{ nI + \sum_j \sum_i \frac{y_i^2\,A}{4} \right\}\theta^*$$

$$V^* = + \frac{12\,E\,n\,I}{H^3}\,W^* + \frac{6\,E\,n\,I}{H^2}\,\theta^* \tag{30}$$

$$N^* = \frac{n\,E\,A}{H}\,U^*$$

If we now replace eqn. (30) by the corresponding equations for an equivalent uniform beam acted upon by end generalized forces M^*, V^*, N^*, and having effective cross section area A^*, inertia property I^*, and shear coefficient ϕ^*, we can show that the A^*, I^*, ϕ^* (for use in eq. (21)) which correspond to the ETC unit are given as

$$\frac{I^*}{1+\phi^*} = n\,I; \quad A^* = n\,A$$

$$\frac{(4+\phi^*)\,I^*}{1+\phi^*} = 4\left[n\,I + \sum_{j=1} \sum_i \frac{y_i^2\,A}{4} \right] \tag{31}$$

17

so that

$$I^* = n\,I + \sum_j \sum_i y_i^2 A \quad ; \quad \phi^* = \frac{\sum_i \sum_j y_i^2 A}{n\,I} \tag{32}$$

The results for A^*, I^*, ϕ^* can be used in eq. (21) in lieu of A, I, ϕ. It is clear that between the two geometries the only essential difference is in the magnitude of ϕ^*. The considerably larger value of ϕ^* obtained using eq. (32) for the ETC unit (as opposed to eq. (21) for the HCC unit) leads to a much smaller spring rate K_{SHEAR} being obtained for the ETC unit. It remains only to compute a value for I_p for both the HCC and the ETC configurations, and then to apply the simulation to typical in-service units.

The torsional analysis for the HCC unit is based on the classical analysis of St. Venant described in [7] and applied to the cross section of Figure 7. By using the membrane analogy the torsion problem, it can easily be shown that I_p for the HCC construction is simply ([7], p. 278)

$$I_p)_{HCC} = K_1 \left(G\,\frac{t}{c} \right) a^3 b \tag{33}$$

where K_1 is a tabulated function of b/a.

An analysis of the end cross section of the ETC construction using Figure 8, yields

$$I_p^* = I_p)_{ETC} = n I_p + \frac{24(1+v)}{H^2} I \sum (X_K^2 + Y_K^2) \tag{34}$$

where I_p, I are the area polar and bending inertia properties of an individual cell, and n is the total number of cells in the unit.

It should be emphasized that in the above analysis, we have assumed that the ends of the individual tubes are assumed to be connected in such a manner as to enforce the requirement that plane sections remain plane. This requirement may or may not be satisfied in any specific ETC design.

APPLICATION TO TYPICAL CONFIGURATION

We consider the configurations of Figures 3 and 5 for the case b = 124.128" (315.3 cm.), a` = 92.8125" (235.7 cm.) having a 9 x 12 cell arrangement for a total of 108 cells. The support legs are assumed to be four 8" x 12" x 1" (20.4 cm. x 30.5 cm. x 2.54 cm.) plate sections forming a box at each corner. Table 1 shows the spring rates computed for the two units assuming that the material is stainless steel having a Young's Modulus E = 28.3 x 10^6 psi (195 KPa) and the rack height H = 161.125" (409.26 cm.).

Table 1   Spring Rates for Model

Item	HCC	UTC
Area of Cell	4.379 sq. in.	4.652 sq. in.
I_{Cell}	=35.55 in.^{4}	33.56 in.^{4}
I_x^* (Unit)	616926 in.^{4}	654996 in.^{4}
I_y^* (Unit)	346825 in.^{4}	367993 in.^{4}
Area of Unit	472.9 in.^{2}	502.4 in.^{2}
I_p^* (Unit)	111321.8 in.^{4}	14939 in.^{4}
$\emptyset_{y,x}; \emptyset_{y,x}^*$	2.35 ; 1.322	179.71 ; 100.53
$K_{TORSION}$ (Eq. 21)	7.520 x 10^9 in.#/rad	1.009 x 10^9 in.#/rad.
$K_{EXTENSION}$	.8306 x 10^8 #/in.	.8818 x 10^8 #/in.
$K_{SHEAR-Y}$	.1214 x 10^8 #/in.	.294 x 10^6 #/in.
$K_{SHEAR-X}$	.1214 x 10^8 #/in.	.294 x 10^6 #/in.
K_{BX}	.1084 x 10^{12} in.#/rad	.1150 x 10^{12} in.#/rad
K_{BY}	.0609 x 10^{12} in.#/rad	.0646 x 10^{12} in.#/rad
K_{IMPACT} (fa=108)	.715 x 10^6 #/in.	5.084 x 10^6 #/in.
K_S (Eq. (23)	.0925 x 10^8 #/in.	.0958 x 10^8 #/in.
K_H (Eq. (25)	5.971 x 10^8 in.#/rad	5.971 x 10^8 in.#/rad
K_f (Eq. (26)	2.004 x 10^8 #/in	2.004 x 10^8 #/in.

The seismic load time histories used have statistically independent components in the global directions. The particular records used are those from three different plant specifications. (See Figures 9-11 showing one horizontal component).

For the HCC unit, net beam forces and moments are used to compute extreme fiber stresses in the rack and in the supports on the basis of the formula.

$$\sigma = \frac{|N|}{A} + \frac{|M_1|C_1}{I_1} + \frac{|M_2|C_2}{I_2} \tag{35}$$

where A, I_1, I_2 are the appropriate geometric properties for the supports or for the entire rack cross section of the HCC unit. As noted previously, the use of the total cross section properties for rack stress evaluation is justified for the HCC unit since the full cross section is available for shear transfer. The evaluation of stress in the ETC unit requires some additional analysis. The cell whose centroid is at X_c, Y_c in the cross section experiences a direct stress of the form

$$\sigma_0 = \frac{E}{H} \left[(q_{14}-q_3) + Y_c(q_{11}-q_4) - X_c(q_{12}-q_5) \right] \tag{36}$$

Due to bending of the cells in two planes, we have, for a cell of nominal cross section (cxc), at the base of the rack

$$\frac{2\sigma_{BX}}{c} = - \frac{6\,E}{H^2} \left[(q_9-q_2) + X_c\,(q_{13}-q_6) \right]$$
$$- \frac{2\,E}{H} \left[q_{11}-q_4 \right] - \frac{6\,E}{H}\, q_4 \tag{37}$$

20

$$\frac{2\sigma_{BY}}{c} = - \frac{6\,E}{H^2} \left[q_7 - q_1) - Y_c(q_{13} - q_6) \right] + \frac{2E}{H} (q_{12} - q_5)$$

$$+ \frac{6E}{H} q_5 \qquad (38)$$

The maximum rack stress in any cell wall can be constructed, at any time instant, from the expression

$$\sigma_{MAX} = \left| \sigma_0 \right| + \left| \sigma_{BX} \right| + \left| \sigma_{BY} \right| \qquad (39)$$

We emphasize that eq. (39) does not include any local stress effects induced by non-rigidity of the rack base, load transfer between supports and adjacent cells or tubes, etc.

For a given time history of stress in the supports, in the HCC rack cross section, or in the ETC individual cell cross section, a determination of unit structural integrity may be carried out. In accordance with [8], structural integrity may be interpreted as setting limits on forces and moment acting separately or together on a defined cross section. For the HCC construction, the entire rack cross section can be used in the structural integrity evaluation; for the ETC construction, we must examine the cross section of the critical cell.

In addition to stress limitations, adjacent racks must not impact during a seismic event. In the simulation herein, virtual mass effects from gaps between racks have been included based on adjacent rack separation equal to 3" (76.2mm). Therefore, assuming the worst motion of adjacent racks, inter-rack impact is precluded if the maximum corner deflection of the rack in either direction is less than 50% of the rack spacing.

21

To assess the two rack constructions, the following simulations are performed:

Table 2   Simulation Studies

Case	Description	Seismic Load
1	Full rack; COF = .8	Fig. 9 (.302 x 1.5 = Max. G. Level) 15 Sec. Duration
2	Full rack; COF = .2	Fig. 9 (.302 x 1.5 = Max. G. Level) 15 Sec. Duration
3	Full rack; COF = .8	Fig. 10 (.17 x 1.5 = Max. G. Level) 12 Sec. Duration
4	Full rack; COF = .8	Fig. 11 (.15 x 1.5 = Max. G. Level) 20 Sec. Duration
5	Half rack load; COF=.8	Same as case 1
6	Full rack; COF = .8	Fig. 10 (.17 x 2.5 = Max. G. Level) 12 Sec. Duration

Values used for coefficients of friction, .2<COF<.8 are accepted upper and lower bound values. Simulations 1-5 are performed with the seismic input amplified by 1.5 on all three input directions. Simulation 6 is performed with the appropriate seismic inputs amplified by 2.5. Thus, case 6, when compared to case 3 shows the effect of employing different amplifications on the same seismic event. Simulation 5, using a half loaded rack, highlights the effect of rigid body rotation of the rack around the vertical axis. The half loaded cases assume that all cells on one side of the unit diagonal are loaded.   In all cases,

22

structural damping of 2% is assumed at a frequency of 20 HZ. Table 3 summarizes the results obtained for stresses and Table 4 shows the maximum corner displacements and maximum floor loads transmitted by the rack. We may define factors R_i which are limited to the value 1 or 2 for an OBE, or SSE event, respectively [8].

R_1 =   direct stress on a net section/allowable OBE tensile (compressive stress)

R_2 =   gross shear on a net section/allowable OBE shear

R_3 =   maximum bending stress in one plane/allowable OBE value

R_4 =   combined flexure and compression ratio

R_5 =   additional combined flexure and tension (compression) ratio

It has been found from a large number of simulations of different HCC racks that factors R_4 or R_5 usually govern structural integrity in both rack and in support legs. In Table 3, we show only values for R_1, and R_4 or R_5 at the most critical location.

23

Table 5

	Honeycomb Construction				End Connected Tube Construction			
	Rack		Support		Rack		Support	
CASE	R1	R4,R5	R1	R4,R5	R1	R4,R5	R1	R4,R5
1	.002	.081	.385	1.46	.200	1.21	.613	1.898
2	.001	.038	.182	.356	.104	.642	.232	.548
3	.001	.068	.322	.964	.155	.955	.372	1.27
4	.001	.065	.319	.957	.180	1.12	.406	1.35
5	.003	.127	.485	1.93	.123	1.004	.294	1.082
6	.002	.061	.513	1.664	.204	1.322	.499	1.50

Table 4

MAXIMUM RACK DEFLECTIONS/TRANSMITTED LOADS

Case	Honeycomb Construction					End Connected Tube Construction				
	X in.	Y in.	Max.* Flr.Ld. lbs.	Single Leg Ld. lbs.	Impact Load lbs.	X in.	Y in.	Max.* Flr.Ld. lbs.	Single Leg Ld. lbs.	Impact Load lbs.
1	1.175	.084	536600	257700	201400	1.049	1.629	1,280,000	411300	578500
2	.573	.489	232900	121000	138300	1.624	1.55	345,700	156100	241800
3	.187	.086	402200	215900	49370	.499	.753	809,400	257700	357800
4	.111	.064	534800	211600	113100	.624	.568	772,700	297700	350500
5	1.35	1.62	496300	340900	79540	2.145	2.392	602,200	200000	181500
6	.826	.343	611000	309800	216800	.856	1.45	985,500	343100	588300

* Static Load = 184,000# for Cases 1,2,3,4,6

    = 103,300# for Case 5

DISCUSSION AND CONCLUSIONS

From the simulation results, we can draw the following conclusions:

1. An accurate picture of the results can only be obtained using 3-D nonlinear time history analysis regardless of the rack modelled. A large contribution to the maximum rack horizontal displacements can be made during an instant when the rack is only supported on one foot and the seismic loads cause a pivot of the rack about the only remaining contact point.

2. Maximum displacements, with a full rack, may be found when the upper bound coefficient of friction value is used. This can be explained by noting that there is a greater tendency for an individual support leg to stick when in ground contact and therefore the possibility of pivoting during an instant when a single foot is in contact is increased.

3. For the seismic events considered here, stress levels in the supports legs have the same order of magnitude in both HCC and ETC racks.

4. Stress levels in the rack cells, above the base, are significantly higher in the ETC unit than in the HCC unit. The ratio of cell stress levels (ETC/HCC) is 10 to 20 in the simulations considered here. While the levels reported here due to beam type stress resultants may not imply violation of gross failure criteria, it is noted that effects near the supports, and construction details not modelled herein, will certainly induce stress raisers on the computed levels reported here. For example, any flexibility at the rack base plate will cause more load

25

to be shifted to the outermost cells; also, local stress raisers will certainly be imposed on those cells nearest the supports. Therefore, it is prudent to ensure that the rack stress levels in the thin walls of the cells, induced by gross dynamic motions, remain low enough so that stress raisers have minimal effect on unit performance. By the very nature of the construction, stress raisers should tend to be higher in the ETC rack compared to what might be present in the HCC rack; therefore, gross stress levels (prior to inclusion of stress raisers) in the thin walled cells on the order of the allowable stress should be viewed with concern.

5. Because of its increased tendency to slide, the ETC rack generally experiences greater horizontal displacements. For some of the simulations studied herein, inter-rack impact may occur since the predicted maximum displacements exceed fifty percent of the assumed spacing between adjcent racks.

6. The maximum load (static plus dynamic impact) transmitted to the floor from the total number of support feet in contact at any instant is larger with the ETC rack. This is attributed to the increased propensity of the ETC rack to lift off the pool floor, possibly pivot on a single support leg, and subsequently re-contact the floor with a substantial impact.

7. The increased displacements found for the case of the half loaded rack dramatically show the effect of 3-D motions and the potential for rigid body rotations about the vertical axis. It is noted that this effect

26

is substantially affected by the initial assumption on the amount of fuel assembly mass participating in impacts with the cell walls.

On the basis of the above results, we conclude that in general, the HCC rack offers greater safety margins in the rack body, is less prone to excessive displacement, and results in lower dynamic loading on the pool floor. Although the model used herein is relatively simple, it does exhibit the features of the 3-D motion and the expected impacts. In any real design application a more elaborate model would be called for, which accounts for impacts at different levels, additional rack degrees of freedom, etc.. In the study reported on here, however, the simplest model is appropriate since we seek only a comparison of results from two different constructions.

The numerical studies presented in the foregoing point up the significance of inter-cell welding. The longitudinal welds connecting the cells in the honey-comb construction are found to improve the stress levels and kinematic response of the rack significantly over the end connected construction. The difference is certain to be all the more important if consolidated pin storage is contemplated.

REFERENCES

1. Habedank, G., Habip, L.M., and Swelim, H., "Dynamic Analysis of Storage Racks for Spent Fuel Assemblies", Nuclear Engineering and Design", 54, 1979, pp. 379-383.

2. "Spent Fuel Pool Modification for Increased Storage Capacity", Quad Cities Units 1 & 2, Commonwealth Edison Company, N.R.C. Document No. 50-264, 50-265 (June, 1981).

3. Levy, S., and Wilkinson, J.P.D., The Component Element Method in Dynamics", McGraw Hill, 1976.

4. Soler, A.I., and Singh, K.P., "Dynamic Coupling in a Closely Spaced Two Body System Vibrating in a Liquid Medium: The Case of Fuel Racks", 3rd Keswick International Conference - Vibration in Nuclear Plants, May 1982, Keswick, United Kingdom.

5. Fritz, R.J., "The Effect of Liquids on the Dynamic Motions of Immersed Solids", ASME Journal of Engineering for Industry, February, 1972, pp. 167-173.

6. Timoshenko, S.P., Strength of Materials, Vol. 1, 3rd Edition, McGraw Hill, p. 175.

7. Timoshenko, S.P., and Goodier, J., Theory of Elasticity, 3rd Ed., McGraw Hill, New York, 1951, pp. 258-315.

8. ASME Code, Section III, Subsection NF, and Appendix XVII, 1980.

NOMENCLATURE

T	system kinetic energy
Q_i, G_i	generalized internal, external forces.
p_i, q_i	generalized coordinates
N_f, N_z	number of internal force elements, degrees of freedom
$[B]$	coupling coefficient matrix
$[M_E], [M_B]; [M_T]$	mass matrices for extension; bending; and torsion of rack
ρ^*, ρ_v^*	effective mass densities
$A; H$	rack cross section metal area; rack height
m_{bi}, I_x, I_y, I_z	mass and inertia properties of rack base
$U_i(t)$	specified seismic motion of pool floor
M	total mass of fuel assembly
$B_{ij}^{(x)}, B_{ij}^{(y)}, A_{ij}$	fluid coupling coefficients (eqs. (10) and (11)
λ	defined in eq. (12)
M_H	hydrodynamic mass (eq. (18)
f_c	number of cells in fuel rack
f_a	number of cells containing fuel assemblies
h	height of rack support leg
A_s, I_s	metal area, metal inertia of support leg cross section
I^*, A^*, ρ^*, I_p^*	equivalent rack properties for ETC unit
c	side length of a single fuel cell
t	wall thickness of fuel cell

$R_i(i=1,2...5)$ structural integrity factors

E Young's Modulus of rack metal

X_c, Y_c centroid of fuel assemblies moving as a group

X_B, Y_B = OFFSET OF FUEL ASSEMBLY GROUP CENTROID FROM RACK MODULE CENTER.
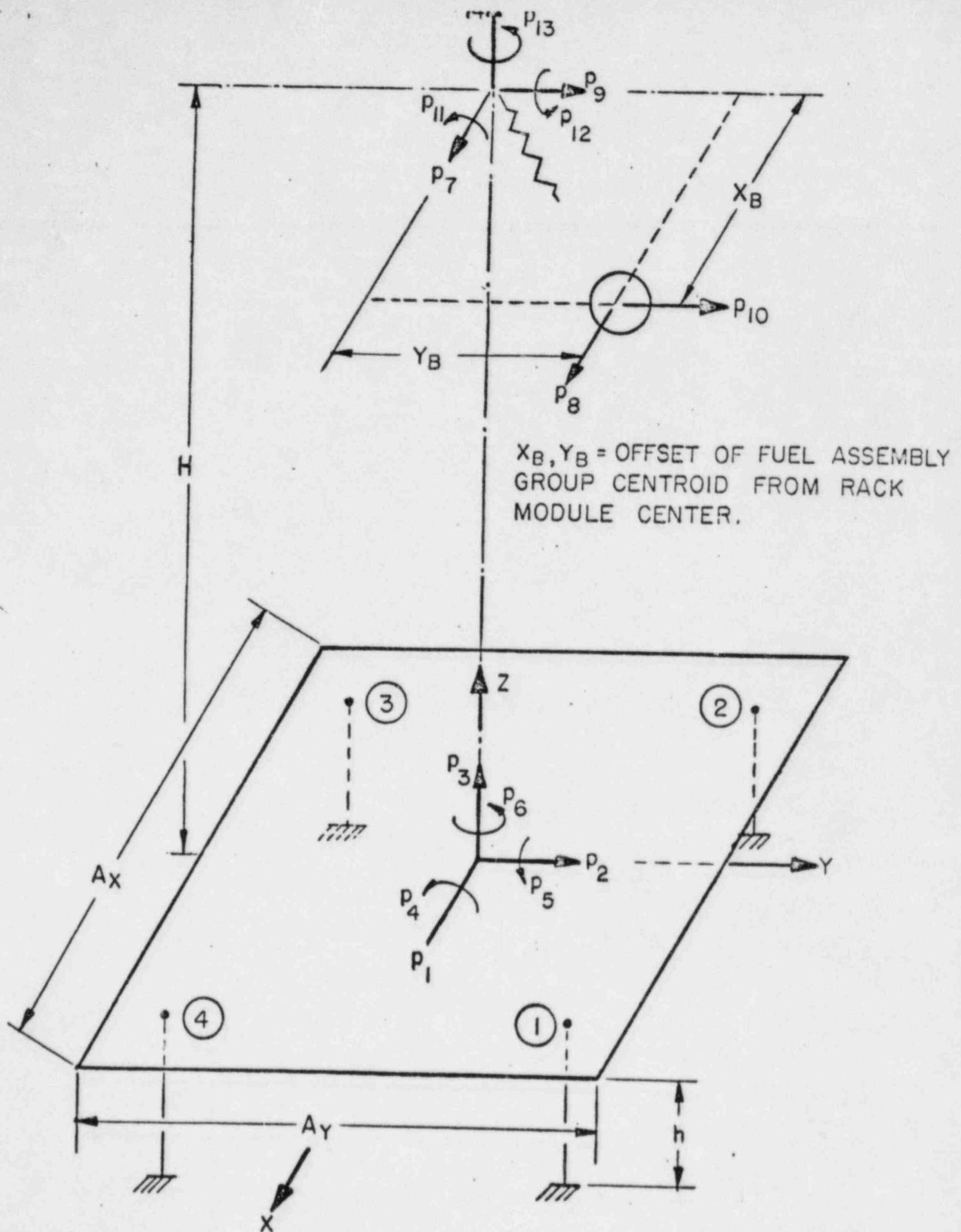
FIG. 1; RACK MODEL SHOWING DEGREES OF FREEDOM
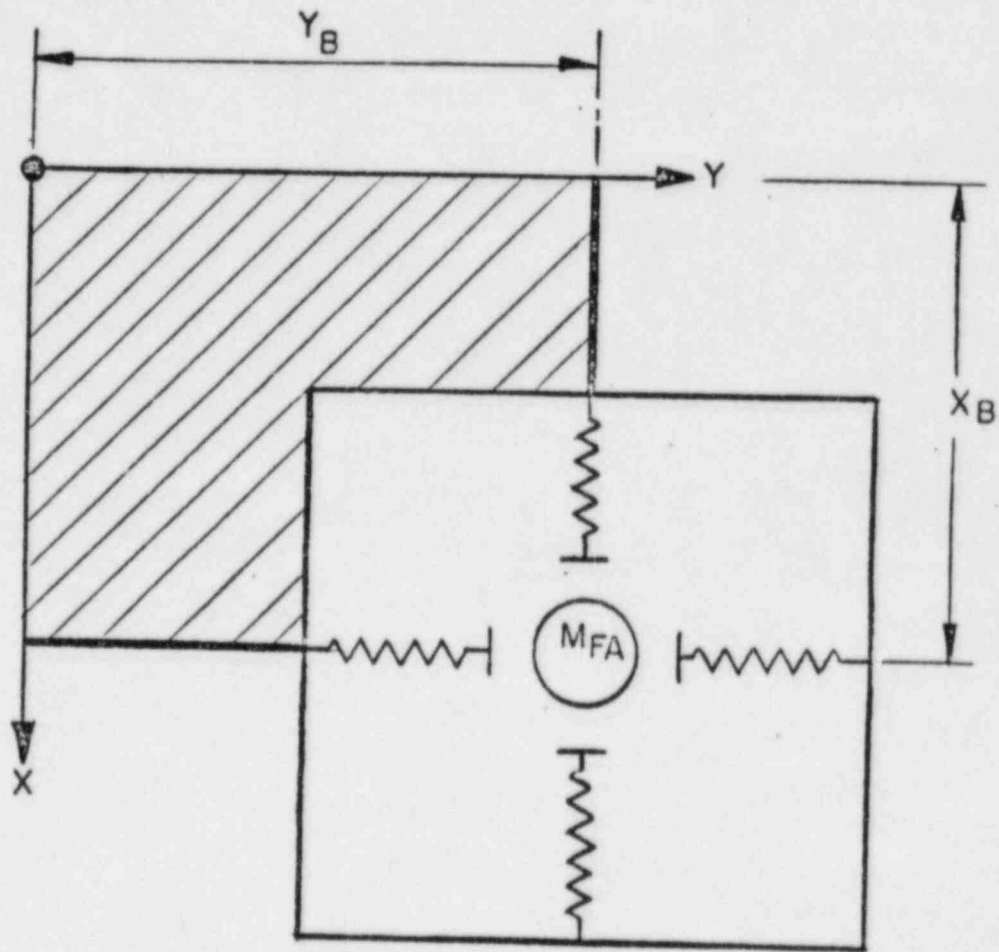
FIG. 2; IMPACT SPRING ORIENTATION AT TOP OF RACK
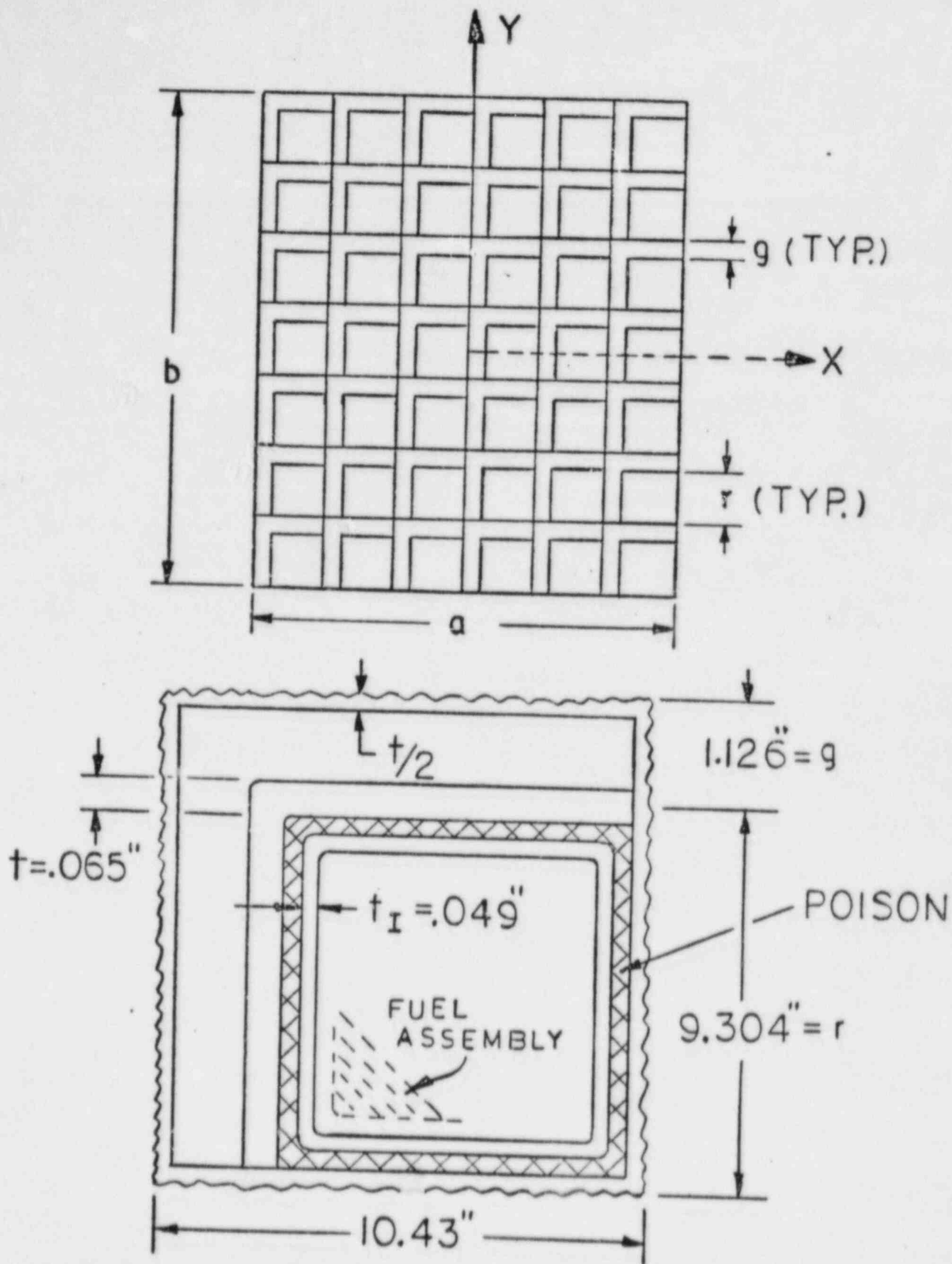
FIG. 3 RACK CROSS SECTION AND TYPICAL CELL GEOMETRY – HONEYCOMB CONSTRUCTION
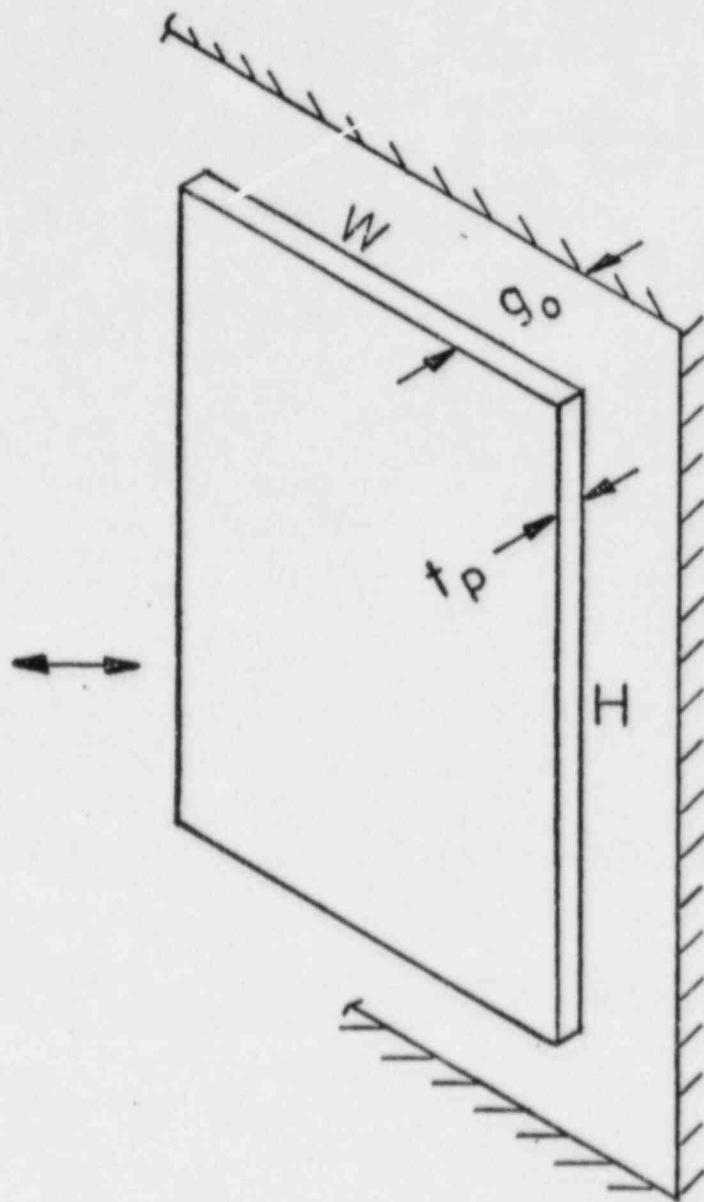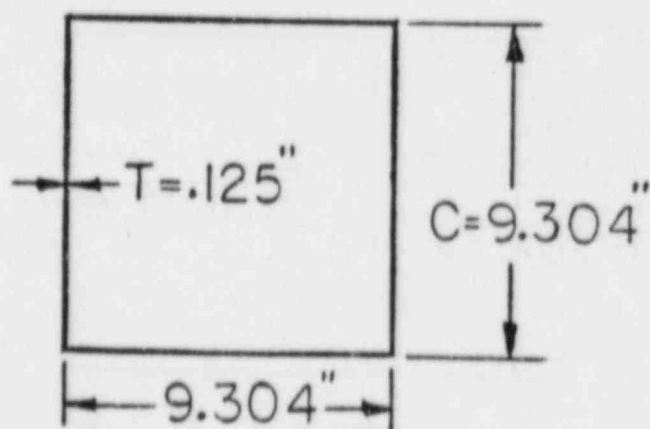
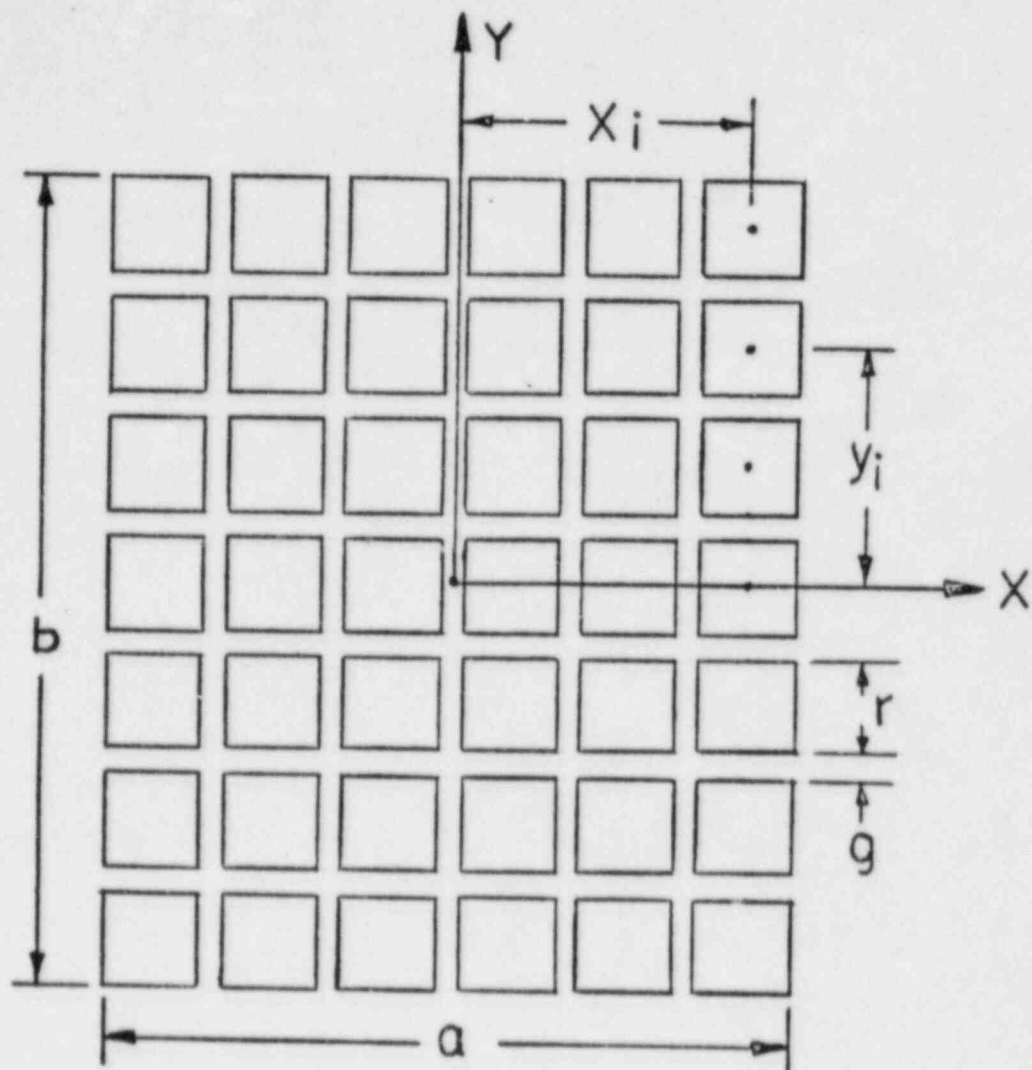FIG. 4   FUEL RACK WALL
MODEL USED TO OBTAIN
FLUID COUPLING

FIG. 5 RACK CROSS SECTION AND
TYPICAL CELL GEOMETRY, UNCONNECTED
TUBE CONSTRUCTION
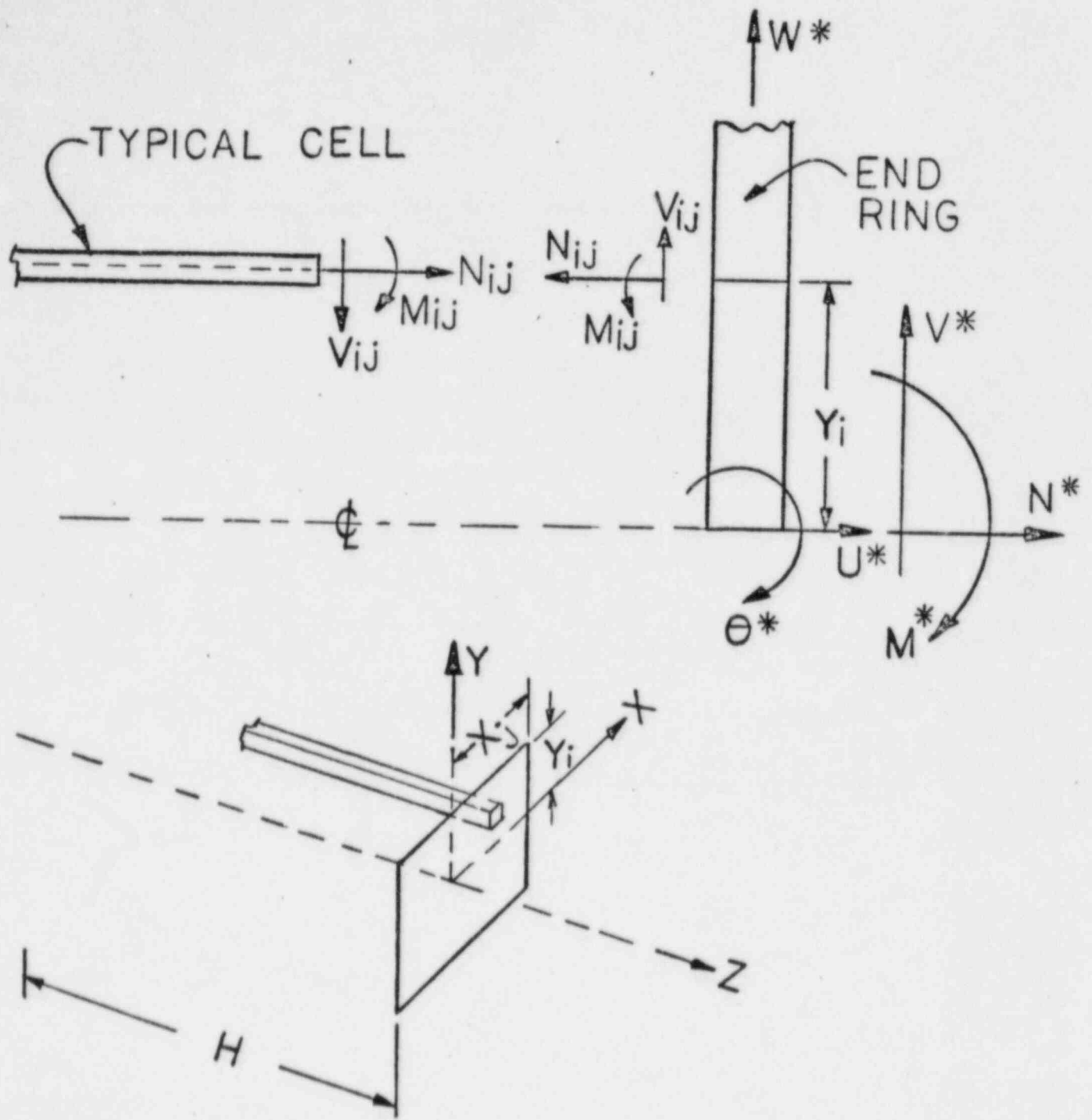
FIG. 6 FREE BODY ANALYSIS OF END RING IN ETC RACK
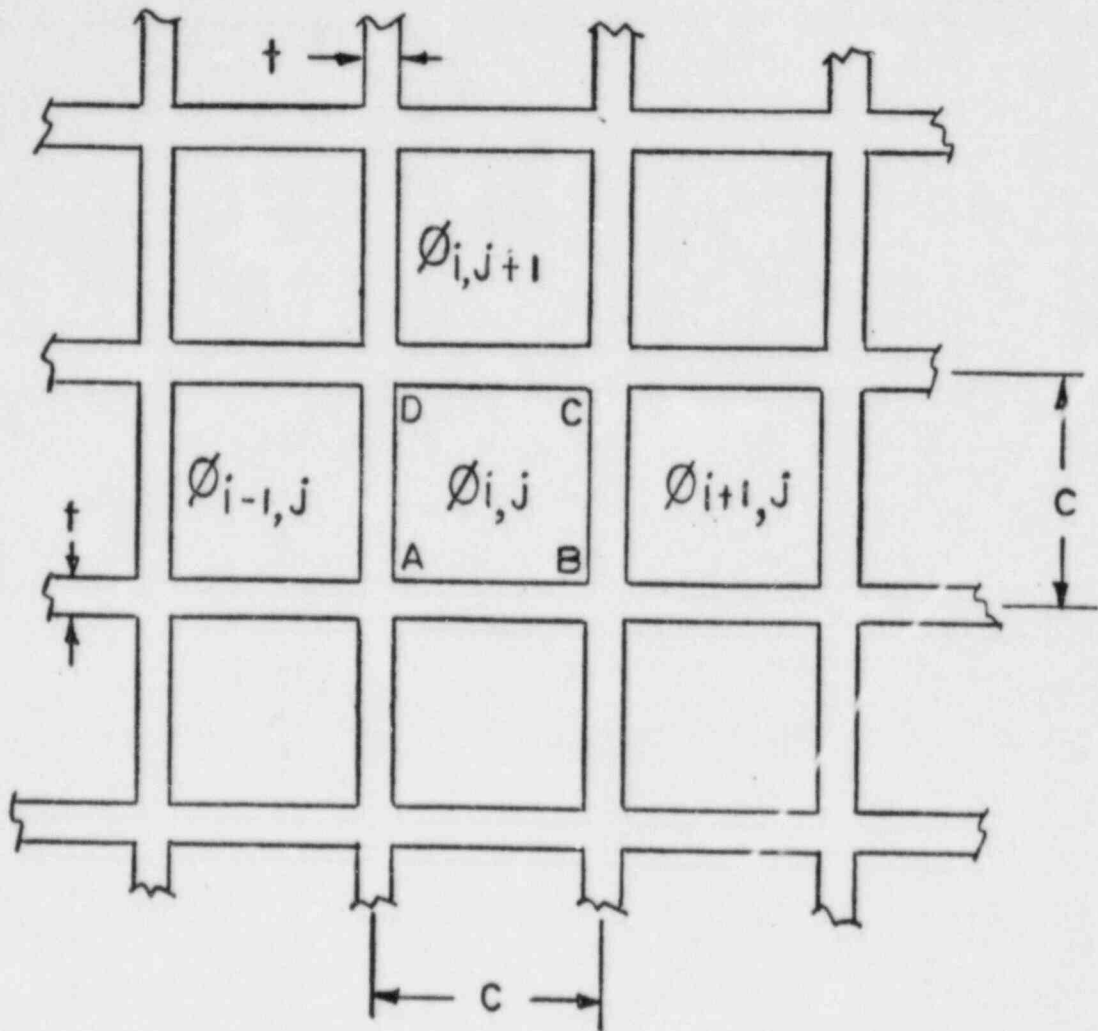
FIG. 7 HCC CROSS SECTION
FOR TORSIONAL RIGIDITY ANALYSIS
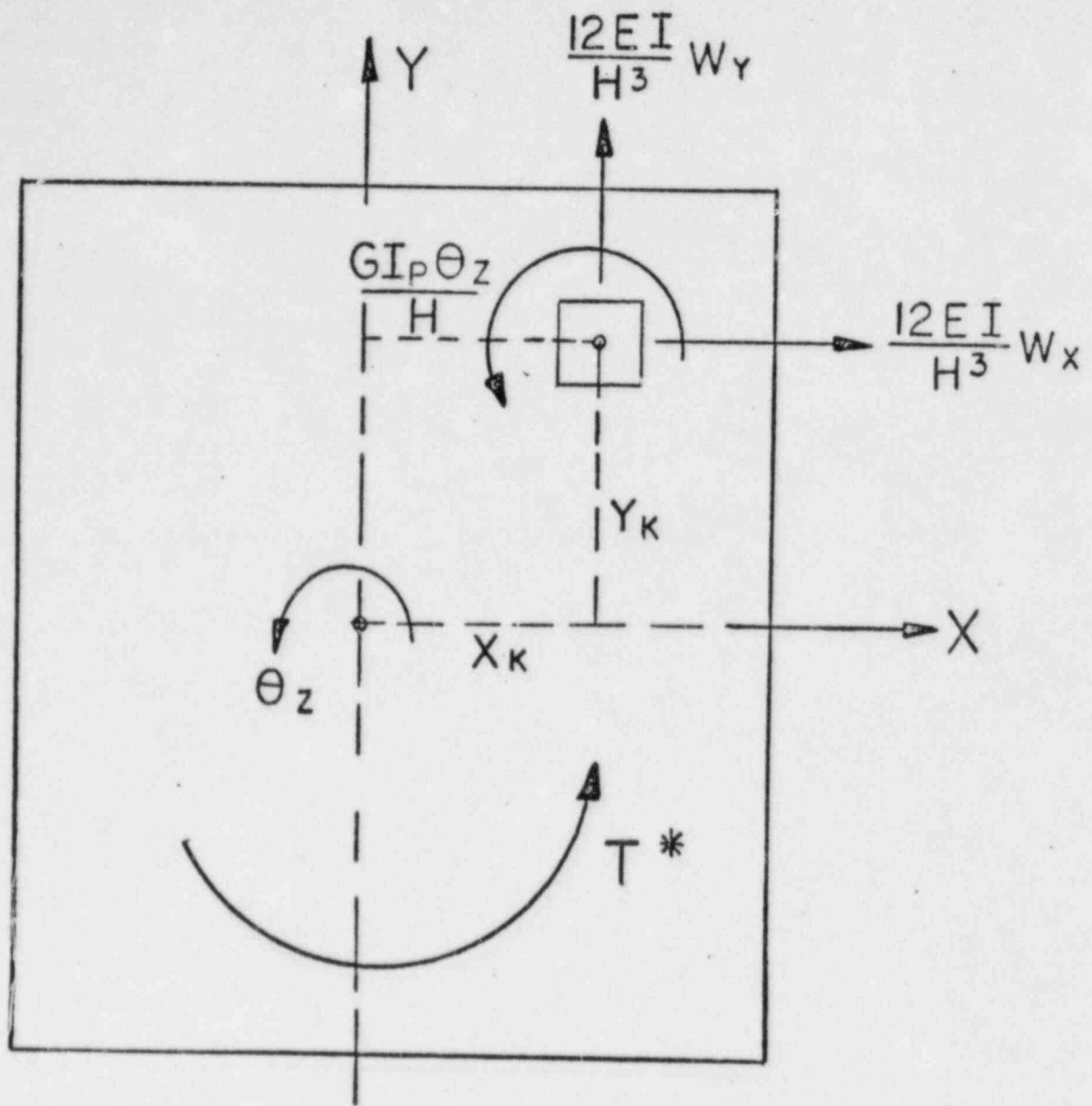
$$T^* = \text{TOTAL CROSS SECTION TORQUE}$$
$$\Theta = \text{ANGLE OF TWIST/UNIT LENGTH}$$

FIG. 8   ETC END CROSS SECTION UNDER TORSION
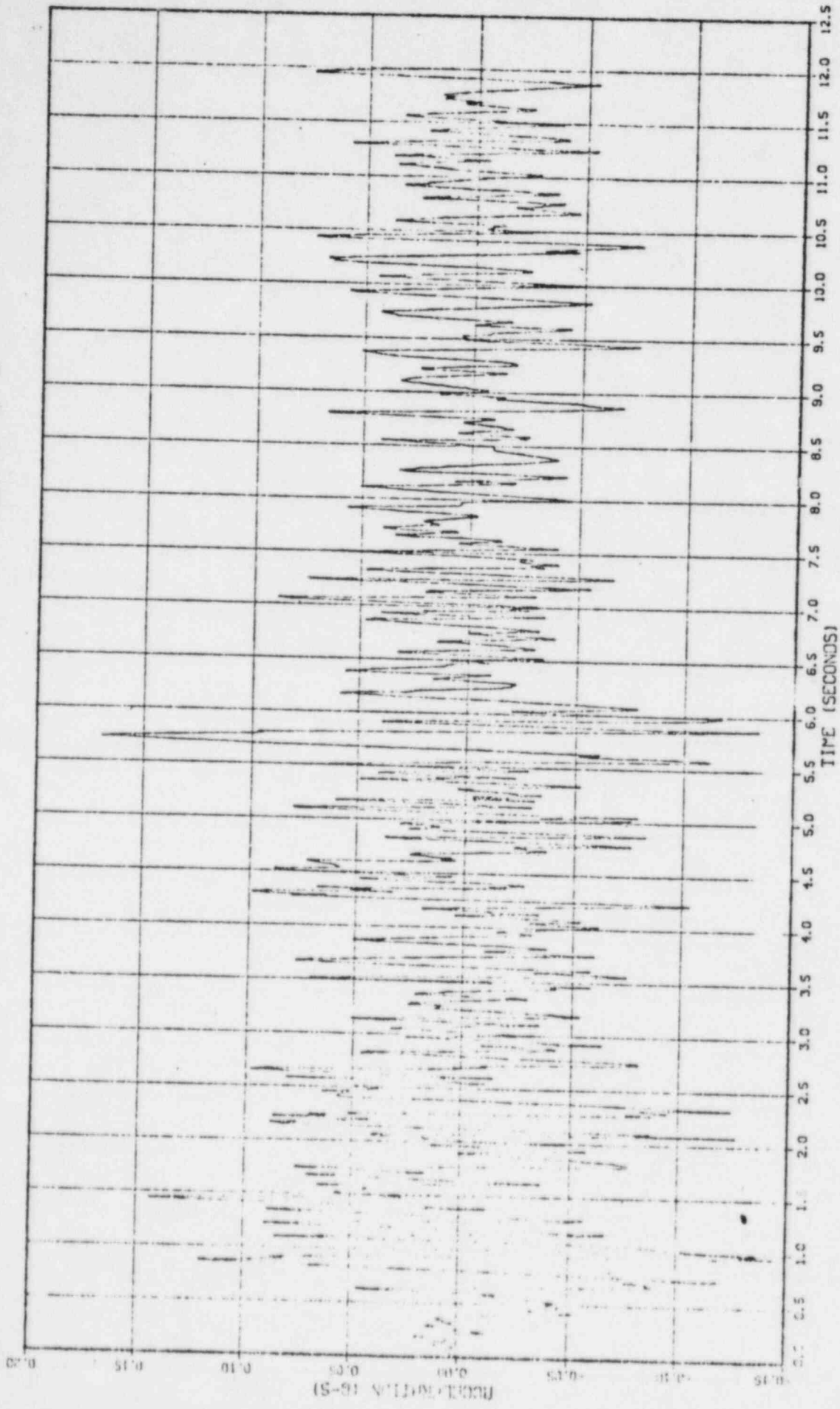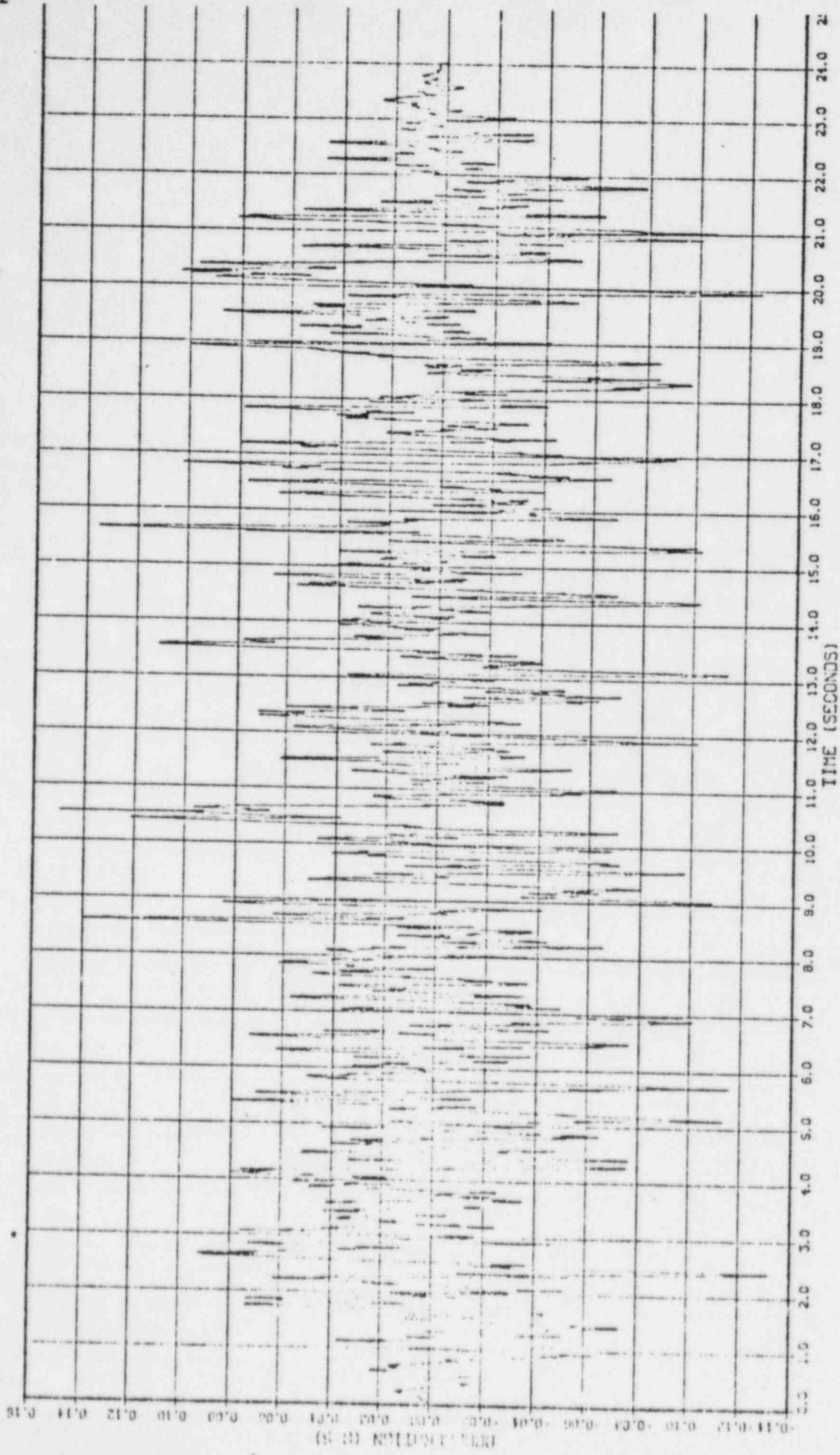
FIGURE 9 - EARTHQUAKE #1
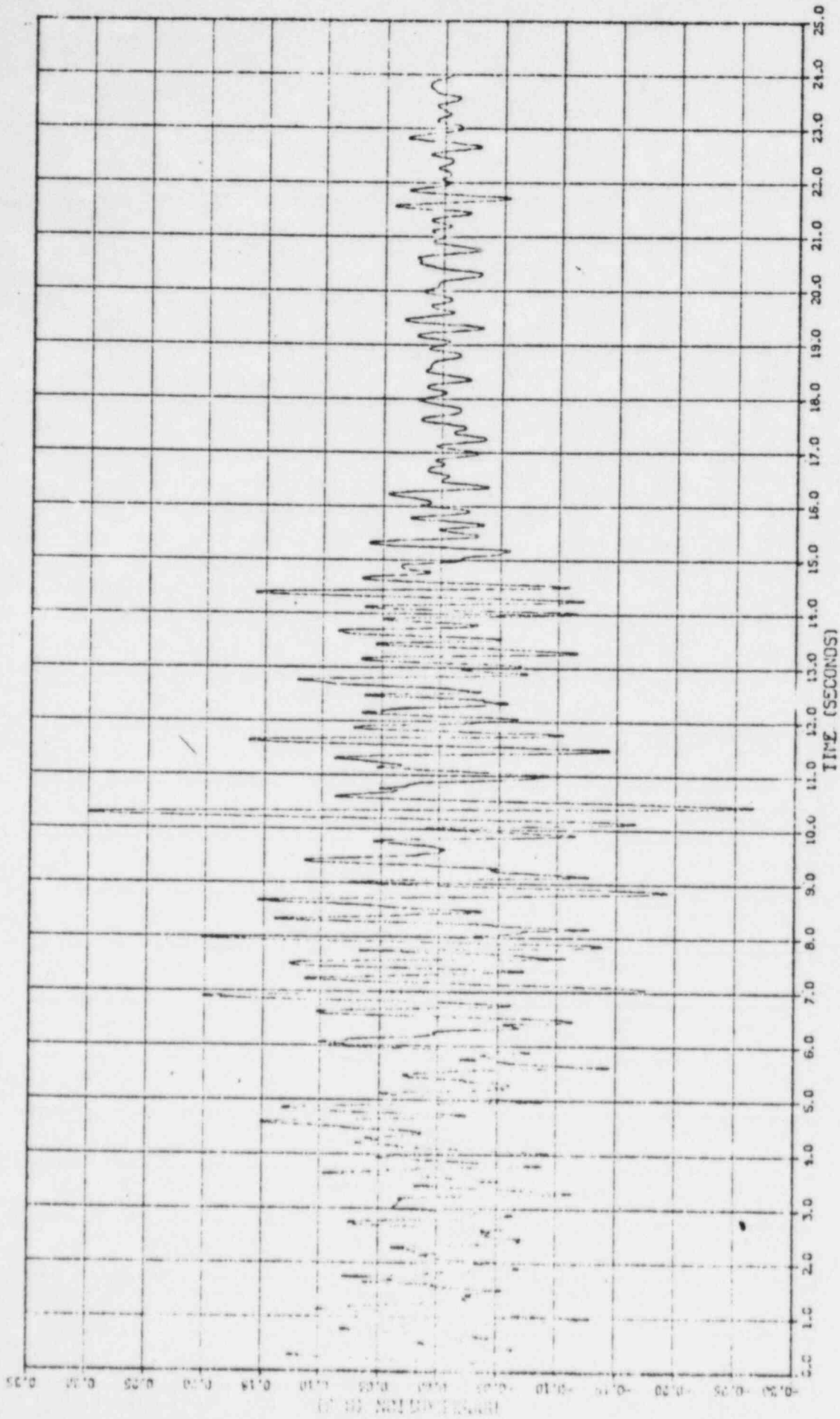
FIGURE IO - EARTHQUAKE #2

TIME (SECONDS)

FIGURE II - EARTHQUAKE "3

MEETING SUMMARY DISTRIBUTION

Docket No(s): 50-395
NRC PDR
Local PDR
NSIC
PRC System
LB #4 r/f
Attorney, OELD
E. Adensam
Project Manager J. Hopkins
Licensing Assistant M. Duncan

NRC PARTICIPANTS

J. Hopkins
G. Lear
P. Kuo
S. Kim
O. Rothberg
J. Lombardo
C. Herrick
T. Belytschko

DESIGNATED ORIGINAL

Certified By _L. Foote_

bcc: Applicant & Service List